A novel platform of RNA 2′-O-methylation high-throughput and site-specific quantification tools revealed its broad distribution on mRNA

Yao Tang[1], Yifan Wu[1], Sainan Wang[1], Xiaolan Lu[1, 4], Xiangwen Gu[1], Yong Li[1], Fan Yang[1], Ruilin Xu[1], Tao Wang[3], Zichen Jiao[3], Yan Wu[1], Liwei Liu[1], Jian-Qun Chen[1]*, Qiang Wang[1]*, Qihan Chen[1, 2, 3]*

1 The State Key Laboratory of Pharmaceutical Biotechnology, School of Life Sciences, Nanjing University, Nanjing, Jiangsu 210023, China.

2 Medical School of Nanjing University, Nanjing, Jiangsu 210093, China.

3 Department of Thoracic Surgery, Nanjing Drum Tower Hospital, The Affiliated Hospital of Nanjing University Medical School, Nanjing, Jiangsu 210093, China.

4 Department of Critical Care Medicine, Nanjing Drum Tower Hospital, The Affiliated Hospital of Nanjing University Medical School, Nanjing, Jiangsu 210093, China.

*Co-corresponding authors

Qihan Chen, Ph.D.

School of Life Sciences, Nanjing University Nanjing,

Jiangsu 210023, China

Phone: +86 13236592587

19 chenqihan@nju.edu.cn

20

21 Qiang Wang, Ph.D.

22 School of Life Sciences, Nanjing University

23 Nanjing, Jiangsu 210023, China

24 Phone: +86 13382014346

25 wangq@nju.edu.cn.

26

27 Jian-Qun, Chen, Ph.D.

28 School of Life Sciences, Nanjing University

29 Nanjing, Jiangsu 210023, China

30 Phone: +0086 025-89682898

31 chenjq@nju.edu.cn.

Abstract

Ribose 2′-O-methylation is involved in critical biological processes, but its biological functions and significance in mRNAs remain largely unknown due to the lack of accurate and efficient identification tools. To overcome this gap, we established NJU-seq (an accurate high-throughput single-base method) and Nm-VAQ (a site-specific quantification tool). We identified thousands of new Nm sites on mRNA of human and mouse cell lines, in which 68 of 84 selected sites were further validated to be 2′-O-methylated more than 1%. Unlike rRNA, the methylated ratios of most validated mRNA Nm sites were lower than 30%. In addition, mRNA 2′-O-methylation was dynamic-changing according to the circumstance, which was presented with MHV infection. Furthermore, Nm sites of lung surgery samples revealed commonness of lung cancer pathogenesis, providing potential new diagnostic markers.

Introduction

More than 100 RNA modifications have been identified, constituting the epi-transcriptome code and affecting RNA functions (Motorin & Helm, 2011). Among these RNA modifications, 2′-O-methylation (otherwise known as Nm), whereby ribose is methylated at the 2′ hydroxyl position without limitation of the base identity, is a widespread RNA modification phenomenon, including multiple RNA types and species (Deryusheva et al., 2012; Jockel et al., 2012; Motorin & Helm, 2011; Tycowski et al., 1996; Zust et al., 2011). Furthermore, several sporadic published studies have demonstrated the importance of 2′-O-methylation in multiple biological processes as an essential signaling regulator. For example, Nm stabilizes the RNA structure by maintaining the ribose C3′-endo conformation, resisting nucleophilic attack, and avoiding 3′-5′ degradation triggered by uridylation (Ji & Chen, 2012; Kawai et al., 1992; Krogh et al., 2016). In addition, a single 2′-O-methylation modification as a molecular tag distinguishes between internal and external RNAs, generates abnormal alternative splicing, and inhibits translation (Ayadi et al., 2019; Daffis et al., 2010; Elliott et al., 2019; Ge et al., 2010; Lalonde et al., 2007; Ma et al., 2014; Zhao & Yu, 2008; Zust et

60 al., 2011). However, despite its potential wide-ranging cellular activities, an in-depth
61 exploration of 2′-O-methylation biological functions are still limited due to the lack of
62 screening tools to detect Nm sites.

63 Three high-throughput Nm detection methods have been developed in the past few
64 years: 2′OMe-seq (Incarnato et al., 2017), RiboMethSeq (Krogh et al., 2016), and Nm-
65 Seq (Dai et al., 2017, 2018). These methods can reliably detect rRNA Nm modification
66 for an abundant amount of rRNA and a high modification ratio. In addition, LC-MS
67 and RTL-P were also used to validate the rRNA site-specific 2′-O-methylation status
68 (Dong et al., 2012; Douthwaite & Kirpekar, 2007). However, the small amount,
69 complex sequence context, and low methylation ratio of mRNAs lead to barriers to the
70 practical application of those methods in mRNAs. To address this problem, we
71 established an accurate high-throughput single-base Nm site screening method NJU-
72 seq and a site-specific 2′-O-methylation quantification tool Nm-VAQ. With the help of
73 these two methods, we efficiently revealed the broad distribution of Nm sites on
74 mRNAs and observed that the 2′-O-methylation ratios of all validated Nm sites on
75 mRNA were lower than 30%.

76 In the previous studies, rRNA was methylated by snoRNP complex, which
77 contained FBL as methyltransferase, NOP56/58, and SNU13 as co-factor, partial
78 complementary snoRNA with conserved C/D box as guide RNA (Yi et al., 2021).
79 Although a particular Nm site on mRNA was reported to be methylated by the same
80 mechanism (Elliott et al., 2019), how the rest of the Nm sites on mRNA methylated
81 remained unknown. On the other hand, viruses such as HIV were reported to be 2′-O-
82 methylated with human FTSJ3, which acts as a methyltransferase, in the host cell
83 (Ringeard et al., 2019). However, further exploration of the whole mechanism relies on
84 accurate Nm site information and methylation ratio evaluation.

85 # Results

86 ## Establishment of NJU-seq

87 Based on the characteristic of 2′-O-methylation, our detection strategy was to take
88 advantage of an Nm-sensitive RNase. Therefore, the newly established NJU-seq relied
89 on helicase and hydrolase activities of RNase R from *Mycoplasma genitalium* (MgR)
90 on ssRNA from the 3′ to 5′ direction, which produced the digested products end at every
91 Nm+1 site (Lalonde et al., 2007). First, A synthesized 22 nt ssRNA substrate carrying
92 one mixed 2′-O-methylation site NmNN (N=A/G/C/U) was incubated with MgR to
93 evaluate its sensitivity to Nm sites (Figure 1A and Appendix figure 1A-B). As expected,
94 the 18 nt ssRNA products accumulated with increasing MgR concentration, confirming
95 the enzyme activity's versatility. In addition, we also performed a reaction of MgR with
96 the synthesized 40 nt ssRNA substrate specifically carrying only the Am site at position
97 28 to demonstrate the exact breakpoint of MgR activity, and the products were TA
98 cloned and sequenced (Appendix figure 1C). Importantly, we discovered that all
99 ssRNA products ended at the Am+1 position (20/20), supporting the detection of Nm
100 sites by the accumulated 3′ end of MgR reaction products. To confirm that the digestion

101 pause was stable in most contexts and may not be affected by certain secondary
102 structures, we incubated an ssRNA with 2′-O-methylation at the 17th position among
103 mixed ribonucleotides (N) from −10 to +10 position with MgR and the products were
104 sequenced by NGS. As shown in Figure 1B, more than 93% of products ended at the
105 Nm+1 position with almost equal ribonucleotides distribution from −10 to −1. In
106 addition, we used multiple ssRNAs with an extended stem region as substrates. As
107 expected, MgR digested all the ssRNA to the Nm+1 position successfully (Appendix
108 figure 1E-F). In addition, an ssRNA substrate with m^6A and m^5C sites downstream of
109 the Am site was incubated with MgR, demonstrating clear products ending at the Nm+1
110 site but nothing at other modification sites (Appendix figure 1D). All the above data
111 indicated that MgR digestion was a great solution to create RNA fragments that ended
112 at the Nm+1 position stably and precisely with no ribonucleotides, context, or
113 secondary structure bias.

114 We combined MgR with NGS to develop a new high-throughput Nm screening
115 method named NJU-seq (Nm-Judged-Universally sequencing). As detailed in the
116 Methods, there were five main steps in NJU-seq (Figure 1C). A sample prepared with

117 the same process without MgR treatment was used as a negative control (NC) group to
118 filter the false-positive outcomes caused by RNA fragmentation bias. First, we tested
119 NJU-seq on total RNA from HeLa cells and analyzed the rRNA results. The sequencing
120 data were aligned to a reference sequence, and reads' 3′ ends were counted (Figure 1D).
121 Comparing rRNA alignments after MgR digestion to NC, 3′ end enrichments
122 correspond to potential Nm sites. For example, between positions 157 to 169 in 18S
123 rRNA, we found that the reads ending at positions 160 and 167 significantly
124 accumulated, indicating two possible Am sites at positions 159 and 166 (Figure 1E).
125 To further evaluate whether other RNA modifications on RNA would affect the activity
126 of MgR, sites' read distributions around all reported sites with eight other RNA
127 epigenetic modifications were browsed, m^6A, pseudouridine (ψ), ac^4C, $m^6{}_2A$, m^1A,
128 m^7G, m^5C, and m^3U (Appendix figure 2 and 3)(Taoka et al., 2018). Based on the
129 results, none of those eight epigenetic modifications caused significant enrichment at
130 1nt downstream or surrounding other position comparing with NC, while Nm sites
131 demonstrated opposite results as expected.

132 We scored each site with the difference of reads end 1 nt downstream divided by
133 reads end just at the target site between MgR treatment and NC group to set a quantified
134 standard (Appendix figure 5). The score was mainly correlated with the copy number
135 of fragments with 2′-O-methylation modification at the Nm site (such as Nm-seq) but
136 not the methylation ratio (such as RiboMethSeq). Candidate Nm sites were further
137 judged by whether reads ending 1 nt downstream of the MgR treatment group were
138 significantly more abundant than the NC group to exclude false-positive results by
139 RNA fragmentation bias. The details of the scoring and filtering steps are described in
140 Methods.

141 **Establish Nm-VAQ as a site-specific validation and quantification tool of Nm**
142 **status**

143 In the previous studies, RTL-P was widely used as a semi-quantification method that
144 can validate sites with high 2′-O-methylation (Dong et al., 2012). However, RTL-P
145 remained several disadvantages, such as hard to validate one site specifically or
146 measure the methylation level accurately, results varying due to the number of targets,
147 or demonstrating potential false positive or negative results (Dong et al., 2012). Here,

148 we hope to develop a method to validate the 2′-O-methylation status of a specific site
149 and acquire the methylation ratio. Hence, we established the Nm-VAQ (an RNase H-
150 based Nm Validation and Absolute Quantification tool) with inspiration from previous
151 relative studies (Yu et al., 1997). Briefly, Nm-VAQ was based on selective cleavage of
152 RNase H and the guidance of a DNA-RNA hybrid probe to target the cleavage site
153 (Figure 2A). With several tests of multiple designs of hybrid probes, we anchored the
154 RNase H cleavage site to the target site with a probe containing 4 DNA and 13 RNA,
155 as shown (Figure 2B and Appendix figure 4A-G). Combined with qPCR, Nm-VAQ
156 quantified the mixed substrates with 2′-O-methylation gradients accurately with much
157 lower methylation ratio (Figure 2C), while RTL-P could only detect Nm sites with
158 modifications higher than 40% (Dong et al., 2012) and presented significantly different
159 results under different conditions (Appendix figure 4H-I). In addition, the tests of Nm-
160 VAQ with 50% 2′-O-methylated substrates at 6.25 fmol, 0.625 fmol, and 0.0625 fmol
161 demonstrated highly consistent results, proving its evaluation capability in low-amount
162 RNA studies (Figure 2D). To date, Nm-VAQ has allowed the study of Nm to the
163 absolute quantification stage.

164 **Mapping of Nm sites of human cell lines**

165 Although our main goal was to identify Nm sites on mRNA, we started from tRNA and
166 rRNA to evaluate the results. As an example, NJU-seq identified Cm_{32} $tRNA^{Gln}$ (UUG)
167 turned out to be consistent with sites reported in previous studies (Marchand et al.,
168 2017), which led to significant fragments accumulation end at 33th position (Appendix
169 figure 6A). On the other hand, 83 Nm sites were identified on rRNA, including 81 Nm
170 sites reported in the previous studies and 2 newly identified (Appendix figure 6B,
171 Appendix table 1). Although NJU-Seq was not as sensitive as RiboMethSeq and LC-
172 MS, it still identified approximate 3/4 of reported Nm sites on rRNA but with high
173 specificity, which was reliable and promising to challenge the Nm identification on
174 mRNA.

175 We next focused on the exploration of Nm sites on mRNAs from HeLa cell lines. With
176 rRNA elimination, the proportion of mRNA in the substrate was substantially increased
177 before MgR treatment. mRNA Nm sites shared with all three independent cell line
178 samples were selected for the following analysis and statistics, as detailed in Methods.

179 The same standard selected the potential Nm sites on mRNA as rRNA, which acquired
180 4074 in HeLa cell lines (Figure 3A and Appendix table 2).

181 Before moving forward to further analysis and statistics of newly identified sites,
182 we wanted to access the rationality of the standard we set and the approximate true
183 positive rate of the 2′-O-methylated sites we selected. Generally, all 4,074 identified
184 mRNA sites of HeLa cell lines were separated into 12 regions with the matrix of the
185 score (30/50/70/90) and fold change (3/5/7) (Figure 3A). 67 sites were selected from
186 the boundary regions of each region as the candidates to be further validated by Nm-
187 VAQ (Figure 3A and Appendix table 2). As shown in Figure 3B, 52 of 67 sites
188 demonstrated 2′-O-methylation ratios higher than 1%, while four negative control
189 unmethylated or methylated by other modification sites demonstrated no positive
190 results by Nm-VAQ. Meanwhile, the *in vitro* transcribed RNA fragments were used to
191 evaluate the potential 2′-O-methylated status of relative sites on *PLXNB2* and *BCL6* by
192 Nm-VAQ as a negative control, which did not produce any false positive signal
193 (Appendix figure 7A). Besides, the *in vitro* transcriptome, which is similar amounts and
194 composition of mRNA but with almost no modification, had been served as a negative

195 control in RNA m^6A modification detection tools to confirm the specificity of identified
196 modification sites (Liu et al., 2022). Here, the mRNA site scores of *in vitro*
197 transcriptome were significantly lower than those identified Nm sites of the template,
198 indicating the high correlation of NJU-seq with Nm modification (Appendix figure 8).
199 The methylation ratios of all selected sites were lower than 30%, much lower than sites
200 in rRNA (Appendix figure 6C and Figure 3B). By calculating the proportion of sites
201 with methylated ratios of each region and different standards, the specificity remained
202 higher than 75% no matter which score threshold or fold change range we used (Figure
203 3C). Hence, NJU-Seq was confirmed to be a reliable method to screen potential Nm
204 sites with pretty high accuracy.

205 We also selected 5 Nm sites on HeLa mRNA with high scores as targets for RTL-
206 P validation; only three showed positive results compared with *GAPDH* as a negative
207 control (Appendix figure 9A). Since the mRNA 2′-O-methylation status of most sites
208 may be much lower than rRNA and RTL-P was limited by false positive, false negative,
209 semiquantitative and non-single nucleotide resolution defects, Nm-VAQ was more
210 appropriate in the following study than RTL-P.

211 We next applied NJU-seq on the other two cell lines, HEK293T and A549, and
212 acquired 2,059/2,367 mRNA Nm sites. 1,044 mRNA Nm sites were shared among all
213 three cell lines (Figure 4A). Three Nm sites shared by three cell lines were selected for
214 further validation: *BCL6* (3, 187,721,452, Gm), *PLXNB2* (22, 50,290,219, Gm), and
215 *TBX2* (17, 61,401,930, Cm). Nm-VAQ confirmed their methylation and evaluated 2′-
216 O-methylation ratios as 0.4-18% (Figure 4B). All validated sites demonstrated clear 2′-
217 O-methylation status but were much lower than Nm sites on rRNA. In addition, we
218 performed GO enrichment analysis of genes with 3-cell-line-shared Nm sites and could
219 see their extensive involvement in various biological processes (Appendix figure 10A).

220 To identify the overall distribution of 2′-O-methylation, we analyzed the sequence
221 composition around the Nm site. We found that Nm modification occurred in a distinct
222 pattern on different ribonucleotides but was similar among the three cell lines (Figure
223 4C). Although A on mRNA may act as a branch point in the intron part and regulate
224 alternative splicing by its 2′-O-methylation status (Zhao & Yu, 2008), more 2′-O-
225 methylations were modified on C and G than A and U. We found high GC content
226 around the Nm sites in the three cell lines, especially G, which might indicate

227 modification bias (Appendix figure 9B). When we further calculated Nm-1 and Nm+1
228 ribonucleotides with Nm together as a tri-ribonucleotide unit, the results showed an
229 apparent uneven distribution with a clear enrichment of UGmU among all three cell
230 lines (Figure 4C).

231 **2′-O-methylation is involved in mRNA alternative splicing events and translation**

232 To identify the potential functions of 2′-O-methylation modifications, we analyzed
233 Nm′s distribution patterns in different functional mRNA regions. By exploring the 2′-
234 O-methylation distribution pattern on mRNA transcripts, we found that in the three cell
235 lines, Nm numbers were CDS>3′UTR>5′UTR, which demonstrated the highest density
236 in the 5′UTR considering the length (Figure 4D). To further investigate the Nm site
237 distribution, we focused on the start and stop codons (Appendix figure 9C-D). 3,479
238 HeLa Nm sites on mRNAs that could cover −50 to +500 nt around the start codon were
239 selected to count the distribution in 50nt-wide windows. Similarly, 3,074 HeLa Nm
240 sites were selected to evaluate the stop codon's −500 to +500 nt regions. Interestingly,
241 both areas demonstrated apparent downward trends of Nm sites from 5′ to 3′ direction.
242 Such a pattern was also seen in the other two cell lines.

243 Such results implied that there were relatively stable patterns of Nm distribution
244 in the functional regions of mRNA. Next, we compared the translation efficiency of
245 genes with and without 2′-O-methylation (Figure 4E). The translation efficiency was
246 reflected by protein abundance/gene expression. Significantly more genes with Nm
247 site(s) showed higher translational efficiency, which strongly suggests a correlation
248 between Nm sites and translation, confirming the vital role of 2′-O-methylation in
249 translational regulation. Previous studies elucidated that pre-mRNA splicing of *ACT1*
250 was affected by Am modification, so we explored whether Nm sites were extensively
251 involved in mRNA splicing (Zhao & Yu, 2008).

252 Interestingly, there were more Nm sites closer to the 5′ exon boundary than those
253 closer to the 3′ exon boundary, significant in the 0-100 window from the boundary
254 (Figure 4F and Appendix figure 9E,G). Such discoveries positively indicated the
255 involvement of 2′-O-methylation in mRNA splicing. To further demonstrate the effects
256 of splicing, we assigned mRNA Nm sites as constitutively spliced exons (CSEs) or
257 alternatively spliced exons (ASEs) (Ge et al., 2010; Ryan et al., 2012). The total length
258 of ASE and CSE with modifications was counted, and the density of Nm sites was

259 obtained. We found that more Nm sites were significantly located in the CSE than in
260 the ASE when considering their different lengths (Figure 4G and Appendix figure
261 9F,H). Such results suggested the importance of 2′-O-methylation in the occurrence and
262 regulation of splicing during mRNA maturation.

263 **2′-O-methylation dynamic response to virus infection**

264 As Nm sites were associated with gene functions, it was interesting to explore whether
265 mRNA 2′-O-methylation participates in gene regulation in response to external stimuli.
266 Therefore, we designed virus infection experiments to observe the dynamic change in
267 Nm sites. We first selected the mouse neuroblastoma (Neuro-2a) cell line as a target to
268 explore mRNA 2′-O-methylation changes before and after mouse hepatitis virus (MHV)
269 A59 infection as a model of viral infection response (Figure 5A). Based on the same
270 standard as the previous parts, 2,272 and 2,549 Nm sites were identified from Neuro-
271 2a cell lines with or without MHV infection, among which 496 Nm sites specifically
272 appeared in the infection group (Figure 5B and Appendix table 3).

273 Together with the results of RNA-Seq, all sites and the relative mRNA expression
274 were divided into nine groups with MHV-infection specific/shared/non-infection

275 specific and expression down-regulated/unchanged/up-regulated as shown (Figure 5B
276 and Appendix figure 10B-C). Five sites were selected to evaluate its 2′-O-methylation
277 status and expression change further. Among them, the methylation ratios of *Pard3*
278 (8:127,610,491, Cm), *Ttyh2* (11:114,690,284, Um), *Tra2b* (16:22,246,081, Um) and
279 *Cnga3* (1:37262191, Gm) showed no obvious change, while the methylation ratio of
280 *Atpaf1* (4:115,811,466, Cm) increased from 9.8% to 14.1% (Figure 5C-D).

281 Based on the principle of NJU-Seq, the results were affected by both methylation
282 status and expression change. For example, the expression level of *Atpaf1* remained no
283 apparent change, while the methylation ratio increased by about 4%, which led to a
284 significant increase in the NJU-seq score. On the other hand, the methylated ratio of
285 *Cnga3* remained at approximately 20%, but the score by NJU-seq increased
286 dramatically due to 4 times more up-regulated mRNA expression (Figure 5D).

287 **Nm demonstrated significant different patterns in normal and lung cancer tissues**

288 Since the viral infection was a transient change, we further explored the dynamics of
289 2′-O-methylation in chronic diseases. Here, we used eight lung cancer clinical samples
290 (6 lung adenocarcinoma (LUAD) and 2 lung squamous cell carcinoma (LUSC)) as a

291 chronic disease response model. NJU-seq was performed to study Nm site differences
292 in lung cancer tissues compared to distant normal lung tissues. As indicated, normal
293 tissue-specific Nm sites were more often present in only 1 to 3 samples, while cancer
294 samples had more shared Nm sites, implying the commonness of lung cancer
295 pathogenesis (Figure 6A and Appendix figure 10D). Such cancerous-specific mRNA
296 Nm sites are ideal candidates as diagnostic markers and are essential in future cancer
297 studies (Figure 6B, Appendix figure 11D-I, and Appendix table 4). For instance,
298 *CDH22* encodes the transmembrane protein cadherin-like protein 22, crucial in
299 metastasis or the spread of cancer (Aydin et al., 2019; Piche et al., 2011). Cm
300 (20:46,174,611) located in *CDH22* CDS was detected in all eight cancer samples but
301 not distant normal samples with no correlation to mRNA expression differences.

302 Further analysis of cancer-specific Nm sites revealed that Nm sites might regulate the
303 molecular function of cancer gene mRNAs in multiple ways. As mentioned above, Nm
304 is closely related to splicing, so we focused on regulating the splicing complex.
305 Interestingly, several Nm sites located upstream of the alternative splicing site can be
306 found, regulating alternative splicing products. For instance, the *NCAM1* gene is

307 involved in cell growth, differentiation, and migration (Sasca et al., 2019). Um
308 (11:113,263,177) on *NCAM1* mRNA was detected in 4 LUAD and 2 LUSC samples
309 located on the 3′ boundary of transcript NCAM1-211 (Figure 6C). We examined all six
310 transcripts covering this site (NCAM1-207, 211, 214, 228, 229, 230) to verify the
311 association between the Um site and splicing. Among 6 LUAD samples, the expression
312 ratio of 5 longer transcripts was lower in 4 LUAD samples with Nm than in 2 samples
313 without Nm, suggesting that 2′-O-methylation modification was associated with
314 alternative splicing to regulate the mRNA products (Figure 6D and Appendix figure
315 11J-M).

316 **Discussion**

317 The 2′-O-methylation modification of RNA ribose affects diverse biological processes.
318 Thus, high-throughput identification for comprehensive and accurate profiling of Nm
319 sites is vital for further research on cellular regulation and functions of 2′-O-
320 methylation. Three high-throughput Nm detection methods have been developed in the
321 past few years: 2′OMe-seq (Incarnato et al., 2017), RiboMethSeq (Birkedal et al., 2015;
322 Erales et al., 2017; Krogh et al., 2016), and Nm-Seq (Dai et al., 2017, 2018) (Table 1).
323 Based on this principle, 2′OMe-seq and RiboMethSeq could identify Nm sites with
324 abundant amounts and high methylation ratios with very good sensitivity such as most
325 Nm sites on rRNA, but various and inconsistent results on Nm sites with lower
326 methylation ratio. For example, 18S 354U was ~20% 2′-O-methylated, which was
327 identified as methylated in 2016 by 2′OMe-seq, but the opposite by RiboMethSeq
328 (Incarnato et al., 2017; Krogh et al., 2016). Such challenge was also seen on 18S 1440
329 Cm, which was not reported until 2020 (Krogh et al., 2020). Based on our results, the
330 methylation ratio of almost all tested mRNA Nm sites was lower than 30%, which
331 indicated that most Nm sites on mRNA were unable to be detected by 2′OMe-seq and

332 RiboMethSeq. On the other hand, the Nm-seq method demonstrated improved mRNA
333 Nm site detection direct targeting to mRNA molecules with 2′-O-methylation (Dai et
334 al., 2017, 2018), similar to our new method NJU-seq. However, two main problems
335 remained and were solved by NJU-seq: 1) Nm-seq based on multiple cycles of
336 OED+RNA purification to enrich the Nm signal, which resulted in a massive loss of
337 RNA content and took at least 16 hours. For NJU-seq, enrichment of the Nm+1 site can
338 be accomplished with only 30 min MgR digestion for only one reaction with much less
339 RNA sample. 2) Ligation bias of fragments. After Nm-seq treatment, the 3′ end of the
340 RNA was 2′-O-methylated, resulting in a much lower ligation efficiency than fragments
341 without oxidation process (Saikia et al., 2006). Thus, some Nm sites were insufficient
342 to obtain more sequencing reads than surrounding non-modified sites. The RNA
343 fragment of NJU-seq ended at the Nm+1 site without 2′-O-methylation, which has no
344 bias in the ligation step. Those shortages may limit the use of Nm-seq in subsequent
345 studies.

346 To observe the specificity and sensitivity of NJU-seq, we knocked known rRNA
347 2′-O-methyltransferase fibrillarin (*FBL*) by siRNA in the HeLa cell line as reported in

348 the previous study (Elliott et al., 2019; Erales et al., 2017). Although *FBL* knockout
349 was proved to be lethal, siRNA could lower the expression of *FBL*, which led to a small
350 decrease of rRNA 2′-O-methylation (Erales et al., 2017). As expected, *FBL* mRNA
351 expression was significantly decreased that confirmed by RT-qPCR (Appendix figure
352 12A). After normalization to total rRNA-aligned reads, fragments ending 1 nt
353 downstream reported Nm sites in the *FBL*-KD group were significantly fewer than
354 those in the untreated group (Appendix figure 12B-C). Such results supported that NJU-
355 seq can reflect the copy number of fragments with 2′-O-methylation. Besides, the
356 methylation levels of several selected sites previously reported as Nm sites between the
357 HeLa negative control and *FBL*-KD groups decreased by 8-20%, as quantified by Nm-
358 VAQ (Appendix figure 12D).

359 The site-specific Nm validation and quantification method Nm-VAQ was another
360 new tool established in this study to fulfill the Nm quantification gap in the study of 2′-
361 O-Methylation. Several previously developed low-throughput Nm detection methods,
362 including LC-MS, RTL-P, and DNA polymerase, have various defects (Aschenbrenner
363 & Marx, 2016; Dong et al., 2012; Douthwaite & Kirpekar, 2007). LC-MS is labor-

364 intensive and difficult for mRNA Nm detection due to the requirement for a large
365 number of RNA molecules (Douthwaite & Kirpekar, 2007). Both RTL-P and DNA
366 polymerase relied on Nm blocking on reverse transcription, which can be called RT-
367 based methods (Aschenbrenner & Marx, 2016; Dong et al., 2012). Any Nm site
368 between the amplification products will generate a methylation signal, and thus, these
369 two detections are non-site-specific methods. Meanwhile, although both RTL-P and
370 DNA polymerase methods could acquire linear results correlated with the methylation
371 ratio with synthetic RNA, the result varied with different amounts of target RNA. As
372 we observed in the evaluation of 18S 1391Cm, the results were significantly different
373 in three RNA amounts, making it difficult to accurately evaluate the 2′-O-methylation
374 ratio of the actual target (Appendix figure 4I). In addition, the original study of RTL-P
375 mentioned false positive and negative results, which may be caused by RNA secondary
376 structures that can occur on several rRNA sites (Dong et al., 2012). Nm-VAQ
377 demonstrated apparent advantages compared to those methods, as listed in Table 2.
378 Nm-VAQ anchored the cleavage position to the target site directed by the chimera and
379 discriminated 2′-O-methylated RNA from unmethylated RNA molecules by RNase H.

380 This method simultaneously acquired the absolute amount of accurate 2′-O-methylation
381 of the target site. In addition, Nm-VAQ showed its capability to consistently evaluate
382 targets with low amounts or low methylation ratios, demonstrating its capability to
383 study the status of specific Nm sites and their dynamic changes.

384 In the data process, we set two parameters score and fold change as 30+ and 3+
385 with a higher standard to maintain a high true positive rate of the screened Nm sites,
386 which was later confirmed to be higher than 75% by Nm-VAQ. More restricted
387 parameter would theoretically result in higher true positive rate, which means both
388 parameters could be adjusted due to the purpose of the study. Although some screened
389 sites were proved to be methylated with lower than 1%, the amount of methylated
390 fragments was not negligible considering their high expression level (Appendix figure
391 7B), which might play essential roles in cell metabolism. Furthermore, NJU-seq
392 achieved high consistency in mRNA duplicate samples (Appendix table 2 and
393 Appendix table 3). These results indicated the stable broad-spectrum applicability of
394 NJU-seq in detecting Nm modification in various RNA molecules with high complexity
395 and low content.

396 In this study, we identified approximate 3/4 previous reported as well as two new
397 Nm sites on rRNA of HeLa cell line. 18S 354U and 1440C were further validated to be
398 2′-O-methylated with ratio lower than 50%, which may be hard to detect consistently
399 by RiboMethSeq and LC-MS. By screening the snoRNA database, 18S 1320G and
400 1784G could be targeted by snoRNA117 and snoRNA116-4, which need further
401 validation in the future study. On mRNA, thousands of new Nm sites were uncovered
402 on mRNAs from humans and mice, installing multiple areas (UTR/CDS, CSE/ASE),
403 revealing its broad distribution. Unlike Nm sites on rRNA, all tested Nm sites on
404 mRNA were 2′-O-methylated at less than 30%, which was hard to answer whether such
405 low methylation ratios could regulate biological processes widely. However, based on
406 previous studies, m^6A were proved to be modified with a median modification ratio of
407 ~40% that was enough to regulate the function of mRNA (Liu et al., 2022; Liu et al.,
408 2013). On the other hand, NJU-seq and Nm-VAQ studied a group of cells from cell
409 lines or tissues, it was unclear whether all cells demonstrated such low modification or
410 some cells were highly methylated while others were not, which required other methods
411 to explore further. A similar distribution pattern of 2′-O-methylation was shared in

412 different cell lines. The non-random distribution of Nm sites and the occurrence of 2′-
413 O-methylation were tightly regulated in critical functional regions, suggesting that Nm
414 might be an essential regulatory means. Thus, 2′-O-methylation modifications played
415 an essential role in mRNA metabolism. In contrast to m^1A with enrichment in the start
416 codon or m^6A with accumulation around the stop codon (Dominissini et al., 2016; Li et
417 al., 2016; Meyer et al., 2012), the Nm distribution pattern was more complicated than
418 these two RNA modifications and may possess broader biological functions. Consistent
419 with Nm-Seq results, we did not discover any conserved motif for mRNA 2′-O-
420 methylation (Dai et al., 2017, 2018). Such results implied mRNA 2′-O-methylation
421 went through a different pathway than sequence-specific 2′-O-methylation on rRNA by
422 FBL/snoRNA or structure-specific 2′-O-methylation on tRNA/miRNA/piRNA by
423 FTSJ and HENMT1 (Liang et al., 2020; Marchand et al., 2017). Based on the novel
424 platform demonstrated in this study, the distribution and quantification of Nm sites were
425 acquired broader and easier, which provide an important basis for the follow-up
426 mechanism exploration.

427 Based on the limited results, it was interesting that 2′-O-methylation might affect
428 the interaction between mRNA molecules and proteins by affecting binding. According
429 to previous studies, 2′-O-methylation could affect RNA-protein interactions by
430 changing the binding surface and space (Jockel et al., 2012; Zust et al., 2011). Since
431 AGO-miRNA-mRNA regulation is one of the most well-known mechanisms, we
432 further analyzed the potential interaction between the RNA-induced silencing complex
433 (RISC) and Nm sites in an infected Neuro-2a cell line. In the MHV-infected Neuro-2a
434 cells, Gm (15:5,097,989) of *Card6* mRNA was located upstream of the cleavage site
435 precisely in the target area of mmu-miR-3073a-3p (Appendix figure 11A-C and
436 Appendix figure 13A,C), which may inhibit RISC cleavage, as reported in a previous
437 study (Martinez & Tuschl, 2004). *Card6* belongs to the CARD gene family, is induced
438 by interferon in multiple immune cells, regulates the immune response, and plays a vital
439 role in inflammation (Li et al., 2014). In addition, we mimicked the 2′-O-methylation
440 on the target mRNA of RISC based on the RISC-mRNA crystal structure (PDB 6MDZ)
441 and the distances between the relative amino acid and modified ribonucleotides of
442 positions 5, 12, and 20 on mRNA were too short, which may interfere with RISC

443 binding (Appendix figure 13B). In addition, other biological processes relying on
444 RNase H-like RNA endoribonuclease activity would all be inhibited by 2′-O-
445 methylation at particular sites, such as Prp8 in alternative splicing, Dicer in miRNA
446 maturation, and RNase L in RNA cleavage of the immune response (Burke et al., 2019;
447 Fica et al., 2017; Ha & Kim, 2014).

448 With the help of NJU-seq and Nm-VAQ, further studies about the function,
449 modification/de-modification/regulation of 2′-O-methylation could be extended. On the
450 other hand, 2′-O-methylation demonstrated a critical function in environmental
451 response and great potential in disease study, diagnosis, and drug discovery.

452

453 ## Materials and METHODS

454 **Cloning, expression, and purification**

455 The RNase R sequence from *Mycoplasma genitalium* (accession number:
456 WP_009885662.1) was synthesized by GenScript Biotech Co. and inserted into the
457 pET28a vector (+) with digestion and ligation at the NdeI and BamHI sites, followed
458 by confirmation by Sanger sequencing. The plasmid was transferred into *E. Coli*. BL21
459 (DE3) strain. Cells were grown in 1 L LB media under 37 °C. IPTG (0.3 mM) was
460 added to every 1 L medium in a shaker incubator to induce protein expression at 16 °C
461 for 18 h. Cell pellets were harvested and lysed by French press with lysis buffer (50
462 mM Tris-HCl at pH 8.0, 250 mM NaCl, 0.5 mM TCEP), followed by centrifuging at
463 10000 rpm for 1 h. MgR protein was purified by passing through a column Nickle resin
464 (GenScript Biotech Co.) and washed by using 3 column volumes of wash buffer (50
465 mM Tris-HCl at pH 8.0, 250 mM NaCl, 20 mM imidazole, 0.5 mM TCEP), then eluted
466 with elution buffer (50 mM Tris-HCl at pH 8.0, 250 mM NaCl, 100 mM imidazole, 0.5
467 mM TCEP). The elution was concentrated and aliquoted into multiple small tubes and

468 stored at −80 °C for further experiments. Protein was confirmed by SDS–PAGE gel,

469 and its concentration was determined by standard BSA protein on the same gel.

470 ***In vitro* assay of RNA hydrolysis**

471 Nm-modified ssRNA substrate was synthesized by GenScript Biotech Co. (5′6-Fam-

472 UAACC UAUGA AGNNN UNmNNC UC-3′). Briefly, various purified proteins were

473 reacted with 600 ng ssRNA substrate in reaction buffer (20 mM Tris-HCl pH 8.0, 100

474 mM KCl, 0.01 mM $ZnCl_2$) at 37 °C for 30 mins. The reaction was terminated by heating

475 to 85 °C for 10 mins. The products were separated by 20% urea-PAGE, visualized with

476 a ChemiDoc XRS+\UnUniversal alHoodII gel imaging system (Bio-Rad) or Tanon

477 3500, and quantified with ImageJ software. A series of reactions with 400 ng ssRNA

478 were designed to test the range of pH and reaction duration. Subsequently, multiple

479 ssRNA substrates were incubated with 18 μg MgR in a 10 μl reaction (20 mM Tris-HCl

480 pH 8.0, 100 mM KCl, 0.01 mM $ZnCl_2$) at 37 °C for 30 mins to test MgR properties.

481 The ssRNA sequences were as follows: ssRNA substrate with multiple modifications

482 (5′6-Fam-AUACC GCAGC UAGAA UGAmGC Um^{5}CAGA UGm^{6}AAA-3′) and

483 ssRNA substrate with hairpin structure (5′6-Fam-UAGCU CUGGA AAUUC

484 UAGAmG CUAAU ACAAA-3′). Another Nm-modified ssRNA substrate was
485 synthesized by GenScript Biotech Co. (5′-AGCCG CCUGG AUACC GCAGC
486 UAGAA UGAmGC UGAGA UGAAA-3′) to test the consistency of hydrolysis. After
487 reacting with MgR, reaction products were purified by an RNA Clean & Concentrator-
488 5 kit (Zymo Research), followed by 5′ phosphorylation (New England BioLabs),
489 repurification, and adaptor ligation (New England BioLabs). The final products were
490 TA cloned and analyzed by Sanger sequencing. An Nm-modified ssRNA substrate was
491 also synthesized by GenScript Biotech Co. (5′-AGCUA GNNNN NNNNN NNmNNN
492 NNNNN NN-3′) and treated with the above protocol. The final products were high
493 throughput sequencing.

494 **Cell culture, tissue and RNA extraction**

495 HeLa cells, HEK293T cells, A549 cells, and Neuron-2a cells were purchased from the
496 Shanghai Institute of Cell Biology, Chinese Academy of Sciences (Shanghai, China).
497 All cells were grown in Dulbecco's modified Eagle's medium (DMEM) supplemented
498 with 10% fetal bovine serum (FBS), 100 units/ml penicillin, and 100 μg/ml
499 streptomycin at 37 °C with 5% CO_2.

500 Following relevant guidelines and regulations, cancerous and distal noncancerous
501 lung tissue samples were obtained from newly diagnosed lung cancer patients. Nanjing
502 Drum Tower Hospital approved the study, and written consent was obtained from all
503 patients.

504 Total RNA from cells and tissues was extracted by the Qiazol RNA extraction kit
505 (QIAGEN). Extracted total RNA was confirmed by Nanodrop (Thermo Fisher) and 1%
506 agarose gel electrophoresis (Sangon Biotech).

507 **Knockdown of FBL in HeLa cell line**

508 For siRNA experiments, siRNA duplexes were used for fibrillarin silencing: 5′-
509 GUCUU CAUUU GUCGA GGAA-AdTdT-3′ (sense sequence). Control siRNA does
510 not target any human sequence (RiboBio). HeLa cells were transfected using
511 LIPOFECTAMINE RNAIMAX reagent (Invitrogen) according to the manufacturer's
512 instructions and collected after 48 h. *FBL* mRNA expression was quantified by a
513 HiScript II 1st Strand cDNA Synthesis Kit (+gDNA wiper) and ChamQ Universal
514 SYBR qPCR Master Mix (Vazyme Biotech Co., Ltd.) according to instructions. The
515 primers were listed in Appendix table 5.

516 **Viral infection**

517 Neuro-2a cells were infected with MHV strain A59 at a multiplicity of 2 plaque-
518 forming units (p.f.u.) per cell. The infected cells were cultured for 1 h and washed three
519 times with PBS to remove the cell-free virus. The infected cells were harvested after
520 40h.

521 **rRNA elimination**

522 Except for HeLa, HEK293T, and A549 cells, which used 15 μg total RNA, all the other
523 samples were processed with 10 μg. The RNA was diluted to 29 μl, and 1 μl rRNA
524 probe (H/M/R) was added (Vazyme Biotech Co., Ltd.). RNA was hybridized with the
525 probe and heated to 95 °C for 2 min, then gradually cooled to 22 °C at 0.1 °C/s and
526 maintained for 5 min. Next, the rRNA was eliminated by adding 1 μl RNase H (New
527 England Biolabs), 4 μl 10X RNase H buffer, 4 μl DEPC water and incubating at 37 °C
528 for 30 min. Subsequently, the hybridization and RNase H reaction were repeated 5/3
529 times to eliminate the rRNA fragment as much as possible. Finally, the probe was
530 digested by 2 units of DNaseI (New England Biolabs) at 37 °C for 30 min. According

531 to the manufacturer's protocol, the RNA product was purified using VAHTS RNA

532 Clean Beads (Vazyme Biotech Co., Ltd.).

533 **NJU-seq**

534 RNA was fragmented by an RNA fragmentation reagents kit (Thermo Fisher) at 95 °C

535 for 10 mins and then purified by 10 μl 3-M NaOAc (pH 5.2), 24 μl 5-μg/μl glycogen,

536 and 372 μl 96% cold ethanol. For facilitating MgR binding of fragments with complex

537 secondary structures after solubilization in water, every 1 μg RNA solution was ligated

538 with 3 μl 25-μM poly(A)-ssRNA adaptor (pAGCUAAAAAAAAAAAAp, synthesized

539 by GenScript Biotech Co.) at 16 °C overnight. The products were then reacted with 30

540 μg MgR in a 60 μl final volume with 20 mM Tris-Cl (pH 8.0), 100 mM KCl, and 0.01

541 mM $ZnCl_2$ at 37 °C for 30 min. Next, the products were purified by an RNA Clean &

542 Concentration-5 kit (Zymo Research), followed by 5′ phosphorylation (39 μl RNA, 5

543 μl (10X T4 PNK Reaction Buffer), 5 μl ATP (10 mM), 1 μl T4 PNK (3′ phosphatase

544 minus, New England BioLabs)). Finally, we constructed the NGS library using the

545 products from the last step following the NEBNext Small RNA Library Prep Set for

546 Illumina (New England BioLabs) protocol. Fragments smaller than 50 nt were extracted

547 from a 6% PAGE gel and sent for NGS using Illumina X-Ten. The exact process

548 prepared the NC sample (negative control group) without MgR protein.

549 **NGS data analysis and statistics**

550 Nm site detection and various statistical analyses were performed using homemade

551 Perl and R scripts and open-source bioinformatics tools. Adaptors were filtered from

552 raw reads using Cutadapt (Version 2.10). Reads were mapped the reference sequences

553 by Bowtie 2 (Langmead & Salzberg, 2012) (Version 2.3.4). rRNA reference

554 sequences are shown in Appendix table 1, and the transcript reference sequences were

555 from GENCODE release 34 and M25 (Frankish et al., 2019). Only protein-coding

556 transcripts with 'BASIC' tags and without 'cds_start_NF' or 'cds_end_NF' tags were

557 retained. Perl scripts handled alignment results, including filtering low-quality or

558 multiple-hit alignments and calculating each site's reads' end count. The likelihood of

559 2′-O-methylation modification at each site was judged based on the following scoring

560 system.

561 **Scoring 2′-O-methylation modification**

562 As shown in Appendix figure 5, we counted the stacking position of the 3′ end of the
563 reads for the treatment group with MgR digestion (TR) and the control group without
564 digestion (NC). First, normalization correction was performed according to the total
565 aligned reads. Then, scoring was performed for each site on the rRNA and
566 transcriptome reference based on the number of reads ending at the current position (N)
567 and the latter (N+1). The NJU-seq score algorithm was as follows.

568 $$Score = \frac{3'Count(TR_{N+1})}{3'Count(TR_N)} - \frac{3'Count(NC_{N+1})}{3'Count(NC_N)}.$$

569 The average of the three replicates' scores was taken and ranked to complete
570 identification for modifications, and here, we took 30 as a threshold. To prevent some
571 points with a similar high N+1 enrichment in NC from being misclassified, we also
572 required $3'Count(TR_{N+1}) > 3 \times mean(3'Count(NC_{N+1}))$. At this point, we
573 finished processing the NJU-seq data and acquiring the Nm sites for subsequent
574 analysis.

575 **Statistics on genomic features**

576 We mainly used Perl and R scripts to perform tri-ribonucleotide unit statistics,
577 presentation of distribution positions, and alternative splicing region statistics on all
578 Nm sites.

579 Sequence probability logo plots for Nm sites were drawn by the R package
580 *ggseqlogo* (Wagih, 2017). The length-normalized mRNA transcript was obtained by
581 averaging all Nm-located transcripts' 5′UTR/CDS/3′UTR length of each sample. Equal
582 length bins of three regions were taken for Nm site counting in each standard transcript.
583 We counted the distance from the Nm site position to the start and stop codon. ASE and
584 CSE were obtained from the statistics of all alternative splicing events provided in the
585 SpliceSeq database (Ryan et al., 2012).

586 **Quantitation of RNA Nm status by RTL-P method**

587 Two sets of primers were designed for the target site, with the F_U forward primer
588 upstream of the Nm site and the F_D forward primer downstream of the Nm site
589 (Appendix table 5). For rRNA Nm detection, the high dNTP concentration reaction
590 mixture consisted of 5× RT Buffer 4 μl, M-MLV (H-) Reverse Transcriptase (Vazyme

591 Biotech Co., Ltd., 200 U/μL) 1 μl, RNase inhibitor (40 U/μL) 1 μl, RNA 100 ng, RT

592 primer (10 μM) 1 μl, RNase-free H_2O 5 μl, dNTPs (1 mM each) 1 μl. The low dNTP

593 concentration reaction mixture was replaced by dNTPs (2 μM each). Then, the mixtures

594 were incubated at 45 °C for 1 hour and 85 °C for 2 min. The cDNA was diluted 100-

595 fold and subsequently subjected to qPCR, with both F_U and F_D products amplified for

596 each cDNA. For mRNA Nm detection, 1 μg of total RNA was used for further RTL-P

597 tests. RT efficiency and RT fold change were calculated according to the following

598 strategy. RT efficiency=template amount measured by F_U and R/template amount

599 measured by F_D and R. RT fold change=RT efficiency with low dNTPs/RT efficiency

600 with high dNTPs (Dong et al., 2012).

601 **The assay of RNase H cleavage**

602 GenScript Biotech Co synthesized RNA oligonucleotides and chimera probes. Briefly,

603 12.5 pmol 5′-FAM-labeled RNA oligonucleotides were mixed with a 75 pmol chimera

604 probe, heated to 95 °C for 2 min, cooled to 22 °C at 0.1 °C/s, and maintained for 5 min.

605 Next, the hybrid was reacted with 1 μl RNase H (New England BioLabs) at 37 °C for

606 30 min and then heated to 90 °C for 10 min to terminate the reaction. The cleavage

607 products were added to RNA Dye (New England BioLabs), analyzed by 20% UERA-

608 PAGE, and visualized by a ChemiDoc XRS+\UnUniversal alHoodII gel imaging

609 system (Bio-Rad).

610 **Nm-VAQ assay of RNA 2′-O-methylation ratio**

611 Synthetic RNA oligonucleotides with/without Nm were obtained from GenScript

612 Biotech Co., and Sangon Biotech Co. synthesized qRT–PCR primers. All sequences

613 were listed in Appendix table 5. The oligonucleotides with/without Nm were mixed to

614 obtain gradient 2′-O-methylation ratio substrates. Then, $6.25*10^{-2}$ pmol substrate was

615 added to 6.25 pmol D(4)R(13) chimera probe at 95 °C for 2 min, followed by cooling

616 to 22 °C at 0.1 °C/s and 22 °C for 5 min. The products were divided into 2 parts for the

617 following reaction. One mixture contained 5 μl previous product, 1 μl RNase H (New

618 England BioLabs), 1 μl 10X RNase H Reaction Buffer, and 3 μl RNase-free H_2O.

619 RNase H storage buffer was substituted for RNase H to form the other mixture to serve

620 as a blank control, followed by 30 min at 37 °C and 10 min at 90 °C. The products were

621 diluted 50-fold and then used to obtain cDNA by a HiScript II 1st Strand cDNA

622 Synthesis Kit (Vazyme Biotech Co., Ltd.). cDNA was diluted 100-fold, and then qPCR

623 was conducted in a 20 μl reaction mixture containing 10 μl ChamQ Universal SYBR

624 qPCR Master Mix (Vazyme Biotech Co., Ltd.), 0.4 μl F primer, 0.4 μl R primer, 2 μl

625 cDNA, and 7.2 μl H_2O, following the protocol: 30 s at 95 °C, then 40 cycles of 95 °C

626 for 10 s and 60 °C for 30 s. Each cDNA was analyzed in 3 replicates. ΔCT (cycle

627 threshold) = Ct value of RNase H reaction- Ct value of control. The linear relationship

628 between the Nm ratio and ΔCT was obtained by GrapicPrism. The additional 6.25 pmol,

629 0.625 pmol, and 0.0625 pmol substrates with 50% Nm ratio were also assayed (cDNA

630 did not dilute), and ΔCT was obtained. The measured modification ratios were

631 calculated by the above linear relationship.

632 **Quantitation of RNA Nm status by Nm-VAQ method**

633 All primers were obtained from Sangon Biotech Co., and the sequences are shown in

634 Appendix table 6. For rRNA Nm detection, 100 ng total RNA and 6.25 pmol chimera

635 probes (molar ratio of rRNA molecules to chimera probes was ~1:200) were hybridized,

636 followed by RNase H cleavage, reverse transcription, and qPCR (cDNA was diluted to

637 100-fold) according to Nm-VAQ protocol. ΔCT was used to calculate the ratio of

638 modification. In addition, some treatments were adjusted to perform mRNA Nm

639 detection. 2-10 μg of total RNA was used for hybrids, and 4 μl of cDNA was used for

640 the qPCR assay.

641 ***In vitro* transcription**

642 The Nm-VAQ detection DNA fragment of *PLXNB2* (22, 50,290,219, Gm) and *BCL6*

643 (3, 187,721,452, Gm) were obtained by qRT-PCR. The T7 primer (TAATA CGACT

644 CACTA TAGGG) was then added to the DNA fragment by PCR. The DNA fragments

645 were as templates to produce RNA fragments without modifications following the T7

646 High Yield RNA Transcription kit instructions (Vazyme Biotech Co., Ltd.). 1ng of *in*

647 *vitro* transcribed RNA was mixed with 1μg total Arabidopsis RNA, followed by

648 hybridization, RNase H cleavage and reverse transcription according to the Nm-VAQ.

649 The cDNA was amplified by PCR and then the product was detected by electrophoresis.

650 The *in vitro* transcriptome total HeLa mRNA was generated as described in the Zhang

651 et al., study (Zhang et al., 2021). The modification-free mRNAs were then performed

652 NJU-seq process and calculated the score.

653 **The snoRNA target prediction**

654 The C/D box snoRNAs were downloaded from snoPY (http://snoopy.med.miyazaki-
655 u.ac.jp). All 427 C/D box snoRNA were obtained. The efficient target prediction for
656 box C/D snoRNAs was followed by PLEXY (http://www.bioinf.uni-
657 leipzig.de/Software/PLEXY/).

658 **qRT–PCR and calculation of expression of NCAM1 transcripts**

659 1 μg of total RNA was used to obtain cDNA with a HiScript II 1st Strand cDNA
660 Synthesis Kit (Vazyme Biotech Co., Ltd.). cDNA was added to ChamQ Universal
661 SYBR qPCR Master Mix (Vazyme Biotech Co., Ltd.), following the process: 95 °C for
662 30 s, 40 cycles of 95 °C for 10S and 60 °C for 30 s. Each cDNA was assayed in 2
663 replicates. The primer oligos were as follows: (NCAM1-all-F: CAACC TTGGG
664 AGGCA ATTCT), (NCAM1-all-R: ACTGC CATTA AAAAG GGGGC), (NCAM1-
665 others-F: ACCTT GGGAG GCAAT TCTGC), and (NCAM1-others-R: GCAGA
666 AACTT CTCTG TAAAT CTAGC). The standard curve was completed as above.

667 Standards of qRT–PCR amplification products were subjected to gradient dilution.
668 qPCR was completed under standard protocols based on the above reagents and
669 procedures.

670 **RNA-seq**

671 We depleted rRNA from total RNA, fragmented it into ~300 bp fragments, and
672 prepared the library for RNA-seq. After library preparation and pooling of different
673 samples, the samples were subjected to PE150 sequencing on the Illumina NovaSeq
674 6000 platform. Paired-end reads were aligned to the GENCODE M25 genome using
675 Bowtie2. Gene expression statistics were performed using HTSeq (Anders et al., 2015)
676 (Version 1.99.2), and differentially expressed genes were obtained using DESeq2
677 (Love et al., 2014) (Version 1.30.1).

678 **Protein abundance**

679 The HeLa protein abundance data were downloaded from the Protein Abundances
680 Across Organisms (PaxDb, Experiment ID 182) (Geiger et al., 2012; Wang et al., 2015).
681 We used transcriptome expression data from the ENCODE (Davis et al., 2018) portal
682 with the following identifiers: ENCFF796REI and ENCFF846THO, and only kept

683 genes with TPM > 0.2. The 6,881 genes with both protein abundance and mRNA
684 expression were used for subsequent analysis. Among them, the number of Nm-located
685 genes was 1,397.

686 **Gene ontology (GO) enrichment**

687 For functional enrichment analysis, genes containing Nm sites were uploaded to
688 DAVID Bioinformatics Resources (http://david.abcc.ncifcrf.gov). Enriched GO terms
689 were restricted to $P \leq 0.05$.

690 **Simulation of structural models**

691 The influence of 2′-O-methylation on RNA-RISC binding was simulated by PyMOL
692 (Version 2.4). We used the molecular structure of Argonaute2-miR-122 bound to the
693 target RNA (PDB ID: 6MDZ) (Sheu-Gruttadauria et al., 2019) for observation and
694 further simulated the modification at some target RNA sites. The methyl group bond
695 angle was strictly controlled to match the real situation, and the distance to the
696 surrounding amino acids before and after binding was measured.

Data and code availability

All data are available in the National Center for Biotechnology Information (accession nos. SAMN17082771 to SAMN 17082794 and SAMN17121988 to SAMN17122043). In addition, principal analysis codes are available on https://github.com/IvanWoo22/NJU_seq.

Acknowledgments

We are grateful to the High-Performance Computing Center of Nanjing University for performing the numerical calculations on its blade cluster system in this paper. In addition, we acknowledge all members of Dr. Chen Jian-Qun's lab, Dr. Li Shanqing and Dr. Liang Naixin for comments and discussions. We also gratefully acknowledge Dr. Chan Robin, Dr. Zhang Hui, and Dr. Zhou Li for editing the paper.

Funding

This work was supported by the Youth Program of the National Natural Science Foundation of China (31801065), the National Key R&D Program of China (2021YFC2701603), Fundamental Research Funds for the Central Universities (021414380507), and National Natural Science Foundation of China (32170218).

Author contributions

Q.H.C., Q.W., and J.Q.C., designed this research; Y.T., S.N.W., X.L.L., X.W.G., Y.L., F.Y., R.L.X., Y.W., and L.W.L. performed this research; Q.H.C., Q.W., Y.T., and Y.F.W., wrote the manuscript; Y.F.W. and Q.W., analyzed the data; T.W., and Z.C.J., provided the clinical samples and pretreatment.

Competing interests

No competing interests declared.

721 **References**

722 Anders, S., Pyl, P. T., & Huber, W. (2015, Jan 15). HTSeq--a Python framework to work with
723 high-throughput sequencing data. *Bioinformatics, 31*(2), 166-169.
724 https://doi.org/10.1093/bioinformatics/btu638

725

726 Aschenbrenner, J., & Marx, A. (2016, May 5). Direct and site-specific quantification of RNA
727 2'-O-methylation by PCR with an engineered DNA polymerase. *Nucleic Acids Res, 44*(8),
728 3495-3502. https://doi.org/10.1093/nar/gkw200

729

730 Ayadi, L., Galvanin, A., Pichot, F., Marchand, V., & Motorin, Y. (2019, Mar). RNA ribose
731 methylation (2'-O-methylation): Occurrence, biosynthesis and biological functions. *Biochim*
732 *Biophys Acta Gene Regul Mech, 1862*(3), 253-269.
733 https://doi.org/10.1016/j.bbagrm.2018.11.009

734

735 Aydin, M., Aydin, E. B., & Sezginturk, M. K. (2019, Feb 1). Electrochemical immunosensor
736 for CDH22 biomarker based on benzaldehyde substituted poly(phosphazene) modified
737 disposable ITO electrode: A new fabrication strategy for biosensors. *Biosens Bioelectron, 126*,
738 230-239. https://doi.org/10.1016/j.bios.2018.10.051

739

740 Birkedal, U., Christensen-Dalsgaard, M., Krogh, N., Sabarinathan, R., Gorodkin, J., & Nielsen,
741 H. (2015, Jan 7). Profiling of ribose methylations in RNA by high-throughput sequencing.
742 *Angew Chem Int Ed Engl, 54*(2), 451-455. https://doi.org/10.1002/anie.201408362

743

744 Burke, J. M., Moon, S. L., Matheny, T., & Parker, R. (2019, Sep 19). RNase L Reprograms
745 Translation by Widespread mRNA Turnover Escaped by Antiviral mRNAs. *Mol Cell, 75*(6),
746 1203-1217 e1205. https://doi.org/10.1016/j.molcel.2019.07.029

747

748 Daffis, S., Szretter, K. J., Schriewer, J., Li, J., Youn, S., Errett, J., Lin, T. Y., Schneller, S.,
749 Zust, R., Dong, H., Thiel, V., Sen, G. C., Fensterl, V., Klimstra, W. B., Pierson, T. C., Buller,
750 R. M., Gale, M., Jr., Shi, P. Y., & Diamond, M. S. (2010, Nov 18). 2'-O methylation of the

751 viral mRNA cap evades host restriction by IFIT family members. *Nature, 468*(7322), 452-456.
752 https://doi.org/10.1038/nature09489

753

754 Dai, Q., Moshitch-Moshkovitz, S., Han, D., Kol, N., Amariglio, N., Rechavi, G., Dominissini,
755 D., & He, C. (2017, Jul). Nm-seq maps 2'-O-methylation sites in human mRNA with base
756 precision. *Nat Methods, 14*(7), 695-698. https://doi.org/10.1038/nmeth.4294

757

758 Dai, Q., Moshitch-Moshkovitz, S., Han, D., Kol, N., Amariglio, N., Rechavi, G., Dominissini,
759 D., & He, C. (2018, Mar). Corrigendum: Nm-seq maps 2'-O-methylation sites in human mRNA
760 with base precision. *Nat Methods, 15*(3), 226-227. https://doi.org/10.1038/nmeth0318-226c

761

762 Davis, C. A., Hitz, B. C., Sloan, C. A., Chan, E. T., Davidson, J. M., Gabdank, I., Hilton, J. A.,
763 Jain, K., Baymuradov, U. K., Narayanan, A. K., Onate, K. C., Graham, K., Miyasato, S. R.,
764 Dreszer, T. R., Strattan, J. S., Jolanki, O., Tanaka, F. Y., & Cherry, J. M. (2018, Jan 4). The
765 Encyclopedia of DNA elements (ENCODE): data portal update. *Nucleic Acids Res, 46*(D1),
766 D794-D801. https://doi.org/10.1093/nar/gkx1081

767

768 Deryusheva, S., Choleza, M., Barbarossa, A., Gall, J. G., & Bordonne, R. (2012, Jan). Post-
769 transcriptional modification of spliceosomal RNAs is normal in SMN-deficient cells. *RNA,*
770 *18*(1), 31-36. https://doi.org/10.1261/rna.030106.111

771

772 Dominissini, D., Nachtergaele, S., Moshitch-Moshkovitz, S., Peer, E., Kol, N., Ben-Haim, M.
773 S., Dai, Q., Di Segni, A., Salmon-Divon, M., Clark, W. C., Zheng, G., Pan, T., Solomon, O.,
774 Eyal, E., Hershkovitz, V., Han, D., Dore, L. C., Amariglio, N., Rechavi, G., & He, C. (2016,
775 Feb 25). The dynamic N(1)-methyladenosine methylome in eukaryotic messenger RNA.
776 *Nature, 530*(7591), 441-446. https://doi.org/10.1038/nature16998

777

778 Dong, Z. W., Shao, P., Diao, L. T., Zhou, H., Yu, C. H., & Qu, L. H. (2012, Nov 1). RTL-P: a
779 sensitive approach for detecting sites of 2'-O-methylation in RNA molecules. *Nucleic Acids*
780 *Res, 40*(20), e157. https://doi.org/10.1093/nar/gks698

Douthwaite, S., & Kirpekar, F. (2007). Identifying modifications in RNA by MALDI mass spectrometry. *Methods Enzymol, 425*, 3-20. https://doi.org/10.1016/S0076-6879(07)25001-3

Elliott, B. A., Ho, H. T., Ranganathan, S. V., Vangaveti, S., Ilkayeva, O., Abou Assi, H., Choi, A. K., Agris, P. F., & Holley, C. L. (2019, Jul 30). Modification of messenger RNA by 2'-O-methylation regulates gene expression in vivo. *Nat Commun, 10*(1), 3401. https://doi.org/10.1038/s41467-019-11375-7

Erales, J., Marchand, V., Panthu, B., Gillot, S., Belin, S., Ghayad, S. E., Garcia, M., Laforets, F., Marcel, V., Baudin-Baillieu, A., Bertin, P., Coute, Y., Adrait, A., Meyer, M., Therizols, G., Yusupov, M., Namy, O., Ohlmann, T., Motorin, Y., Catez, F., & Diaz, J. J. (2017, Dec 5). Evidence for rRNA 2'-O-methylation plasticity: Control of intrinsic translational capabilities of human ribosomes. *Proc Natl Acad Sci U S A, 114*(49), 12934-12939. https://doi.org/10.1073/pnas.1707674114

Fica, S. M., Oubridge, C., Galej, W. P., Wilkinson, M. E., Bai, X. C., Newman, A. J., & Nagai, K. (2017, Feb 16). Structure of a spliceosome remodelled for exon ligation. *Nature, 542*(7641), 377-380. https://doi.org/10.1038/nature21078

Frankish, A., Diekhans, M., Ferreira, A. M., Johnson, R., Jungreis, I., Loveland, J., Mudge, J. M., Sisu, C., Wright, J., Armstrong, J., Barnes, I., Berry, A., Bignell, A., Carbonell Sala, S., Chrast, J., Cunningham, F., Di Domenico, T., Donaldson, S., Fiddes, I. T., Garcia Giron, C., Gonzalez, J. M., Grego, T., Hardy, M., Hourlier, T., Hunt, T., Izuogu, O. G., Lagarde, J., Martin, F. J., Martinez, L., Mohanan, S., Muir, P., Navarro, F. C. P., Parker, A., Pei, B., Pozo, F., Ruffier, M., Schmitt, B. M., Stapleton, E., Suner, M. M., Sycheva, I., Uszczynska-Ratajczak, B., Xu, J., Yates, A., Zerbino, D., Zhang, Y., Aken, B., Choudhary, J. S., Gerstein, M., Guigo, R., Hubbard, T. J. P., Kellis, M., Paten, B., Reymond, A., Tress, M. L., & Flicek, P. (2019, Jan 8). GENCODE reference annotation for the human and mouse genomes. *Nucleic Acids Res, 47*(D1), D766-D773. https://doi.org/10.1093/nar/gky955

Ge, J., Liu, H., & Yu, Y. T. (2010, May). Regulation of pre-mRNA splicing in Xenopus oocytes by targeted 2'-O-methylation. *RNA, 16*(5), 1078-1085. https://doi.org/10.1261/rna.2060210

Geiger, T., Wehner, A., Schaab, C., Cox, J., & Mann, M. (2012, Mar). Comparative proteomic analysis of eleven common cell lines reveals ubiquitous but varying expression of most proteins. *Mol Cell Proteomics, 11*(3), M111 014050. https://doi.org/10.1074/mcp.M111.014050

Ha, M., & Kim, V. N. (2014, Aug). Regulation of microRNA biogenesis. *Nat Rev Mol Cell Biol, 15*(8), 509-524. https://doi.org/10.1038/nrm3838

Incarnato, D., Anselmi, F., Morandi, E., Neri, F., Maldotti, M., Rapelli, S., Parlato, C., Basile, G., & Oliviero, S. (2017, Feb 17). High-throughput single-base resolution mapping of RNA 2-O-methylated residues. *Nucleic Acids Res, 45*(3), 1433-1441. https://doi.org/10.1093/nar/gkw810

Ji, L., & Chen, X. (2012, Apr). Regulation of small RNA stability: methylation and beyond. *Cell Res, 22*(4), 624-636. https://doi.org/10.1038/cr.2012.36

Jockel, S., Nees, G., Sommer, R., Zhao, Y., Cherkasov, D., Hori, H., Ehm, G., Schnare, M., Nain, M., Kaufmann, A., & Bauer, S. (2012, Feb 13). The 2'-O-methylation status of a single guanosine controls transfer RNA-mediated Toll-like receptor 7 activation or inhibition. *J Exp Med, 209*(2), 235-241. https://doi.org/10.1084/jem.20111075

Kawai, G., Yamamoto, Y., Kamimura, T., Masegi, T., Sekine, M., Hata, T., Iimori, T., Watanabe, T., Miyazawa, T., & Yokoyama, S. (1992, Feb 4). Conformational rigidity of specific pyrimidine residues in tRNA arises from posttranscriptional modifications that enhance steric interaction between the base and the 2'-hydroxyl group. *Biochemistry, 31*(4), 1040-1046. https://doi.org/10.1021/bi00119a012

842 Krogh, N., Asmar, F., Come, C., Munch-Petersen, H. F., Gronbaek, K., & Nielsen, H. (2020,
843 Dec). Profiling of ribose methylations in ribosomal RNA from diffuse large B-cell lymphoma
844 patients for evaluation of ribosomes as drug targets. *NAR Cancer, 2*(4), zcaa035.
845 https://doi.org/10.1093/narcan/zcaa035

846

847 Krogh, N., Jansson, M. D., Hafner, S. J., Tehler, D., Birkedal, U., Christensen-Dalsgaard, M.,
848 Lund, A. H., & Nielsen, H. (2016, Sep 19). Profiling of 2'-O-Me in human rRNA reveals a
849 subset of fractionally modified positions and provides evidence for ribosome heterogeneity.
850 *Nucleic Acids Res, 44*(16), 7884-7895. https://doi.org/10.1093/nar/gkw482

851

852 Lalonde, M. S., Zuo, Y., Zhang, J., Gong, X., Wu, S., Malhotra, A., & Li, Z. (2007, Nov).
853 Exoribonuclease R in Mycoplasma genitalium can carry out both RNA processing and
854 degradative functions and is sensitive to RNA ribose methylation. *RNA, 13*(11), 1957-1968.
855 https://doi.org/10.1261/rna.706207

856

857 Langmead, B., & Salzberg, S. L. (2012, Mar 4). Fast gapped-read alignment with Bowtie 2.
858 *Nat Methods, 9*(4), 357-359. https://doi.org/10.1038/nmeth.1923

859

860 Li, L., Chen, W., Zhu, Y., Wang, X., Jiang, D. S., Huang, F., Wang, L., Xiang, F., Qin, W.,
861 Wang, Q., Zhang, R., Zhu, X., Li, H., & Chen, X. (2014, Jul). Caspase recruitment domain 6
862 protects against cardiac hypertrophy in response to pressure overload. *Hypertension, 64*(1), 94-
863 102. https://doi.org/10.1161/HYPERTENSIONAHA.113.03021

864

865 Li, X., Xiong, X., Wang, K., Wang, L., Shu, X., Ma, S., & Yi, C. (2016, May). Transcriptome-
866 wide mapping reveals reversible and dynamic N(1)-methyladenosine methylome. *Nat Chem*
867 *Biol, 12*(5), 311-316. https://doi.org/10.1038/nchembio.2040

868

869 Liang, H., Jiao, Z., Rong, W., Qu, S., Liao, Z., Sun, X., Wei, Y., Zhao, Q., Wang, J., Liu, Y.,
870 Chen, X., Wang, T., Zhang, C. Y., & Zen, K. (2020, Jul 27). 3'-Terminal 2'-O-methylation of

lung cancer miR-21-5p enhances its stability and association with Argonaute 2. *Nucleic Acids Res, 48*(13), 7027-7040. https://doi.org/10.1093/nar/gkaa504

Liu, C., Sun, H., Yi, Y., Shen, W., Li, K., Xiao, Y., Li, F., Li, Y., Hou, Y., Lu, B., Liu, W., Meng, H., Peng, J., Yi, C., & Wang, J. (2022, Oct 27). Absolute quantification of single-base m(6)A methylation in the mammalian transcriptome using GLORI. *Nat Biotechnol*. https://doi.org/10.1038/s41587-022-01487-9

Liu, N., Parisien, M., Dai, Q., Zheng, G., He, C., & Pan, T. (2013, Dec). Probing N6-methyladenosine RNA modification status at single nucleotide resolution in mRNA and long noncoding RNA. *RNA, 19*(12), 1848-1856. https://doi.org/10.1261/rna.041178.113

Love, M. I., Huber, W., & Anders, S. (2014). Moderated estimation of fold change and dispersion for RNA-seq data with DESeq2. *Genome Biol, 15*(12), 550. https://doi.org/10.1186/s13059-014-0550-8

Ma, Y., Wei, Y., Zhang, X., Zhang, Y., Cai, H., Zhu, Y., Shilo, K., Oglesbee, M., Krakowka, S., Whelan, S. P., & Li, J. (2014, Mar). mRNA cap methylation influences pathogenesis of vesicular stomatitis virus in vivo. *J Virol, 88*(5), 2913-2926. https://doi.org/10.1128/JVI.03420-13

Marchand, V., Pichot, F., Thuring, K., Ayadi, L., Freund, I., Dalpke, A., Helm, M., & Motorin, Y. (2017, Feb 9). Next-Generation Sequencing-Based RiboMethSeq Protocol for Analysis of tRNA 2'-O-Methylation. *Biomolecules, 7*(1). https://doi.org/10.3390/biom7010013

Martinez, J., & Tuschl, T. (2004, May 1). RISC is a 5' phosphomonoester-producing RNA endonuclease. *Genes Dev, 18*(9), 975-980. https://doi.org/10.1101/gad.1187904

Meyer, K. D., Saletore, Y., Zumbo, P., Elemento, O., Mason, C. E., & Jaffrey, S. R. (2012, Jun 22). Comprehensive analysis of mRNA methylation reveals enrichment in 3' UTRs and near stop codons. *Cell, 149*(7), 1635-1646. https://doi.org/10.1016/j.cell.2012.05.003

Motorin, Y., & Helm, M. (2011, Sep-Oct). RNA nucleotide methylation. *Wiley Interdiscip Rev RNA, 2*(5), 611-631. https://doi.org/10.1002/wrna.79

Piche, B., Khosravi, S., Martinka, M., Ho, V., & Li, G. (2011). CDH22 expression is reduced in metastatic melanoma. *Am J Cancer Res, 1*(2), 233-239. https://www.ncbi.nlm.nih.gov/pubmed/21969168

Ringeard, M., Marchand, V., Decroly, E., Motorin, Y., & Bennasser, Y. (2019, Jan). FTSJ3 is an RNA 2'-O-methyltransferase recruited by HIV to avoid innate immune sensing. *Nature, 565*(7740), 500-504. https://doi.org/10.1038/s41586-018-0841-4

Ryan, M. C., Cleland, J., Kim, R., Wong, W. C., & Weinstein, J. N. (2012, Sep 15). SpliceSeq: a resource for analysis and visualization of RNA-Seq data on alternative splicing and its functional impacts. *Bioinformatics, 28*(18), 2385-2387. https://doi.org/10.1093/bioinformatics/bts452

Saikia, M., Dai, Q., Decatur, W. A., Fournier, M. J., Piccirilli, J. A., & Pan, T. (2006, Nov). A systematic, ligation-based approach to study RNA modifications. *RNA, 12*(11), 2025-2033. https://doi.org/10.1261/rna.208906

Sasca, D., Szybinski, J., Schuler, A., Shah, V., Heidelberger, J., Haehnel, P. S., Dolnik, A., Kriege, O., Fehr, E. M., Gebhardt, W. H., Reid, G., Scholl, C., Theobald, M., Bullinger, L., Beli, P., & Kindler, T. (2019, May 23). NCAM1 (CD56) promotes leukemogenesis and confers drug resistance in AML. *Blood, 133*(21), 2305-2319. https://doi.org/10.1182/blood-2018-12-889725

929 Sheu-Gruttadauria, J., Pawlica, P., Klum, S. M., Wang, S., Yario, T. A., Schirle Oakdale, N.
930 T., Steitz, J. A., & MacRae, I. J. (2019, Sep 19). Structural Basis for Target-Directed
931 MicroRNA Degradation. *Mol Cell, 75*(6), 1243-1255 e1247.
932 https://doi.org/10.1016/j.molcel.2019.06.019

933

934 Taoka, M., Nobe, Y., Yamaki, Y., Sato, K., Ishikawa, H., Izumikawa, K., Yamauchi, Y., Hirota,
935 K., Nakayama, H., Takahashi, N., & Isobe, T. (2018, Oct 12). Landscape of the complete RNA
936 chemical modifications in the human 80S ribosome. *Nucleic Acids Res, 46*(18), 9289-9298.
937 https://doi.org/10.1093/nar/gky811

938

939 Tycowski, K. T., Smith, C. M., Shu, M. D., & Steitz, J. A. (1996, Dec 10). A small nucleolar
940 RNA requirement for site-specific ribose methylation of rRNA in Xenopus. *Proc Natl Acad*
941 *Sci U S A, 93*(25), 14480-14485. https://doi.org/10.1073/pnas.93.25.14480

942

943 Wagih, O. (2017, Nov 15). ggseqlogo: a versatile R package for drawing sequence logos.
944 *Bioinformatics, 33*(22), 3645-3647. https://doi.org/10.1093/bioinformatics/btx469

945

946 Wang, M., Herrmann, C. J., Simonovic, M., Szklarczyk, D., & von Mering, C. (2015, Sep).
947 Version 4.0 of PaxDb: Protein abundance data, integrated across model organisms, tissues, and
948 cell-lines. *Proteomics, 15*(18), 3163-3168. https://doi.org/10.1002/pmic.201400441

949

950 Yi, Y., Li, Y., Meng, Q., Li, Q., Li, F., Lu, B., Shen, J., Fazli, L., Zhao, D., Li, C., Jiang, W.,
951 Wang, R., Liu, Q., Szczepanski, A., Li, Q., Qin, W., Weiner, A. B., Lotan, T. L., Ji, Z., Kalantry,
952 S., Wang, L., Schaeffer, E. M., Niu, H., Dong, X., Zhao, W., Chen, K., & Cao, Q. (2021, Apr).
953 A PRC2-independent function for EZH2 in regulating rRNA 2'-O methylation and IRES-
954 dependent translation. *Nat Cell Biol, 23*(4), 341-354. https://doi.org/10.1038/s41556-021-
955 00653-6

956

Yu, Y. T., Shu, M. D., & Steitz, J. A. (1997, Mar). A new method for detecting sites of 2'-O-methylation in RNA molecules. *RNA, 3*(3), 324-331. https://www.ncbi.nlm.nih.gov/pubmed/9056769

Zhang, Z., Chen, T., Chen, H. X., Xie, Y. Y., Chen, L. Q., Zhao, Y. L., Liu, B. D., Jin, L., Zhang, W., Liu, C., Ma, D. Z., Chai, G. S., Zhang, Y., Zhao, W. S., Ng, W. H., Chen, J., Jia, G., Yang, J., & Luo, G. Z. (2021, Oct). Systematic calibration of epitranscriptomic maps using a synthetic modification-free RNA library. *Nat Methods, 18*(10), 1213-1222. https://doi.org/10.1038/s41592-021-01280-7

Zhao, X., & Yu, Y. T. (2008, Jan). Targeted pre-mRNA modification for gene silencing and regulation. *Nat Methods, 5*(1), 95-100. https://doi.org/10.1038/nmeth1142

Zust, R., Cervantes-Barragan, L., Habjan, M., Maier, R., Neuman, B. W., Ziebuhr, J., Szretter, K. J., Baker, S. C., Barchet, W., Diamond, M. S., Siddell, S. G., Ludewig, B., & Thiel, V. (2011, Feb). Ribose 2'-O-methylation provides a molecular signature for the distinction of self and non-self mRNA dependent on the RNA sensor Mda5. *Nat Immunol, 12*(2), 137-143. https://doi.org/10.1038/ni.1979

977 **Figures**

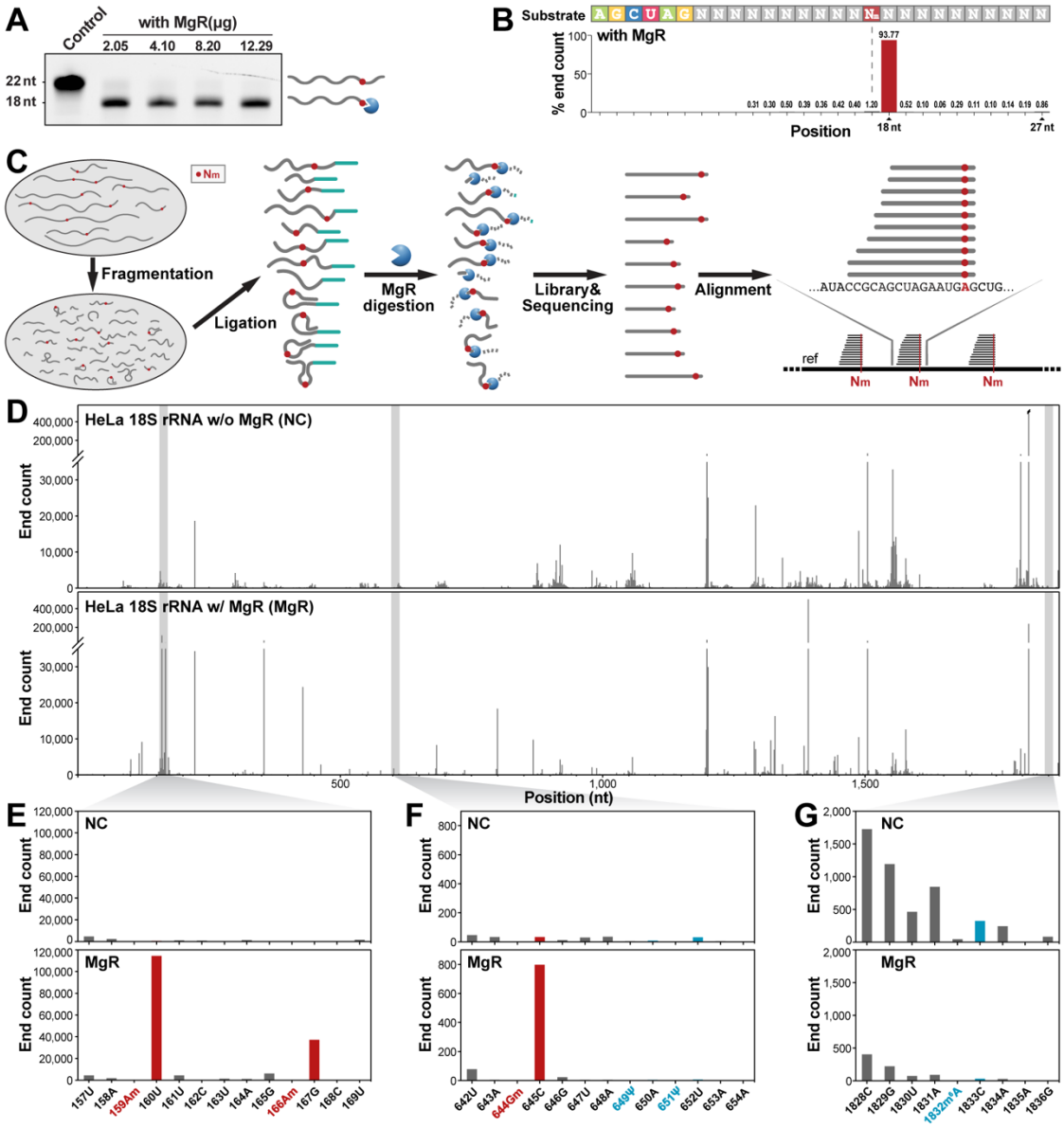

978

979 Figure 1 Establish a novel high-throughput method, NJU-seq, for RNA 2′-O-methylation

980 (A) *In vitro* ssRNA hydrolysis assay. The ssRNA substrate (5′-6-Fam-UAACCUAUGA

981 AGNNNUNmNNC UC-3′, N represents the mix of A/G/C/U) was reacted with varying MgR

982 amounts. The left electrophoresis showed digestion products of MgR, and a schematic was

983 shown on the right.

984 (B) High throughput sequencing of MgR hydrolyzed ssRNA products. The ssRNA substrate

985 (5′-AGCUA GNNNN NNNNN NNmNNN NNNNN NN-3′) was incubated with MgR protein,

986 followed by library construction and NGS. All reads shorter than 27 nt were counted, and the
987 ratios were presented.

988 (C) Schematic workflow of NJU-seq. 1) total RNA fragmentation; 2) 3′ tail ligation; 3) RNase
989 R from Mycoplasma genitalium (MgR) digestion; 4) NGS library preparation and high-
990 throughput sequencing; 5) alignment and analysis.

991 (D) Plots showing read 3′ end counts on HeLa 18S rRNA with (MgR, bottom) and without
992 (NC, top) MgR digestion.

993 (E-G) Plots showing read 3′ end counts of regions 157-169, 642-654, and 1828-1836 on 18S
994 rRNA, without and with MgR digestion. Sites marked with red were previously reported as 2′-
995 O-methylated, and blue were previously reported as m^6A or pseudouridine.

996

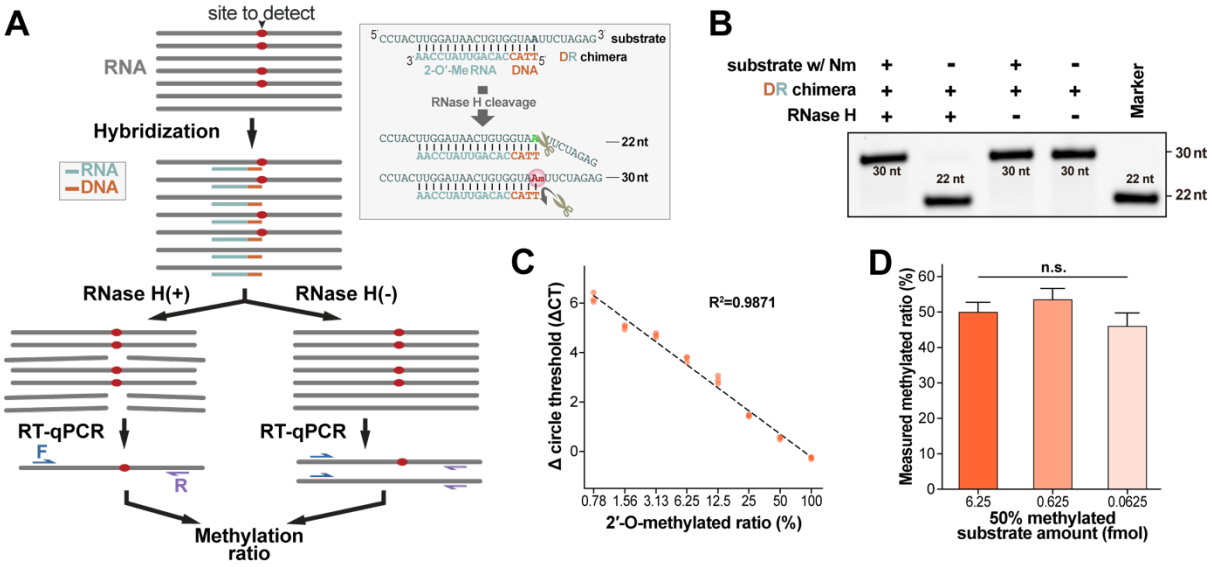

Figure 2 Establish a low-throughput Nm validation tool, Nm-VAQ

(A) Schematic workflow of Nm-VAQ. 1) the hybrid of RNA and chimera probes. In the substrate, the red site indicated the target site was 2′-O-methylated. In the chimera probe, the reddish-brown region showed the DNA, and the light green region showed the 2′-O-methylated RNA; 2) with/without RNase H cleavage; 3) RT-qPCR. The methylation ratio was from ΔCT (cycle threshold) of RNase H cleavage and control sample. The box on the right showed an example of RNase H cleavage directed by the chimera probe in Figure 2B. Hybrid schemes of RNA substrates (up sequences) and chimera probes (down sequences) were shown.

(B) The RNase H reaction products were presented by electrophoresis. The number presented the length of FAM-labeled cleavage products.

(C) Correlation between the 2′-O-methylated ratio of substrate and ΔCT (cycle threshold) for the Nm-VAQ assay. A $6.25*10^{-2}$ pmol substrate with and without Nm was mixed to obtain a known Nm ratio, and ΔCT was obtained from the RNase H treated and control samples.

(D) Measurement of three different substrate concentrations with an Nm ratio of 50%. Nm ratio was calculated with ΔCT. n.s., not significant, by ordinary one-way ANOVA.

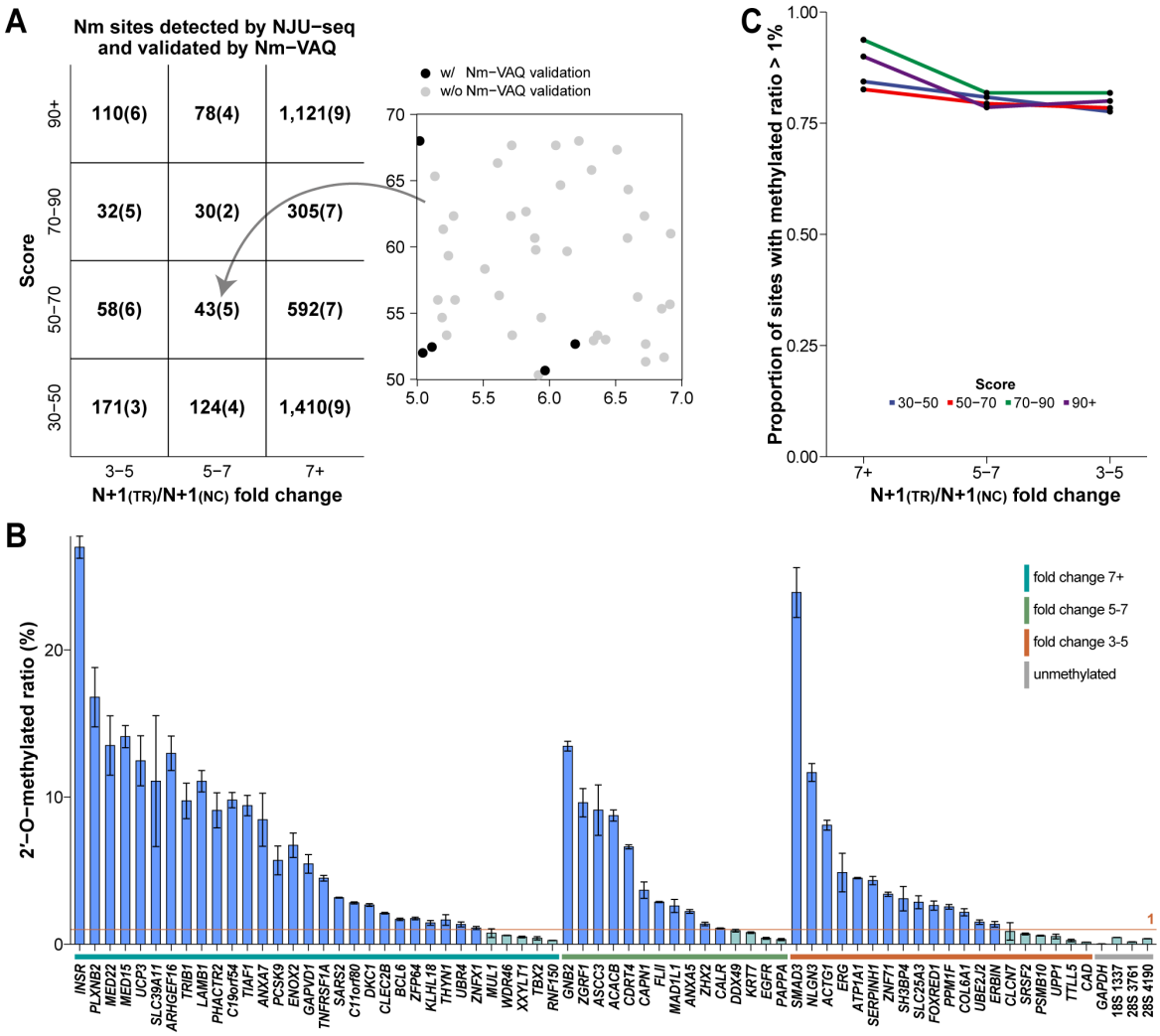

Figure 3 Detection and validation of HeLa mRNA Nm sites by NJU-seq and Nm-VAQ

(A) The distribution of HeLa mRNA Nm sites detected by NJU-seq and validated by Nm-VAQ. 4,074 mRNA Nm sites were screened in criteria the same as for rRNA. All Nm sites were divided into 12 regions based on score and foldchange. Each box represented the number of Nm sites detected by NJU-seq (without brackets) and by Nm-VAQ (in brackets), respectively (left). An example of the selection criteria for Nm-VAQ of Nm sites was shown on the right. As shown in the figure, Nm sites closest to score boundary and sites closest to fold change boundary were subjected to subsequent validation analysis by Nm-VAQ in each box, avoiding any artificial bias in the selection of validation candidates. The black dots indicated the selected sites for the following validation.

1025 (B) The methylation ratio in HeLa mRNA Nm sites detected by Nm-VAQ. The Nm sites are
1026 divided into three ranges of fold change (3-5, 5-7, 7+) and ranked from highest to lowest. The
1027 unmethylated sites on GADPH mRNA (12:6,537,190, G), and 28S 4190A, 3761C, 18S 1337C,
1028 which were reported as m6A, m5C, and ac4C in previous studies were selected as the negative
1029 control. The sites in blue indicated their 2′-O-methylation ratios were higher than 1%, while
1030 the cyan sites were lower methylated. The complete information of all selected sites can be
1031 found in Appendix table 6. Error bars described SEM for three technical replicates.

1032 (C) The proportion of sites with a methylated ratio higher than 1% in different fold change
1033 ranges and score ranges. Each of them was higher than 75%.

1034

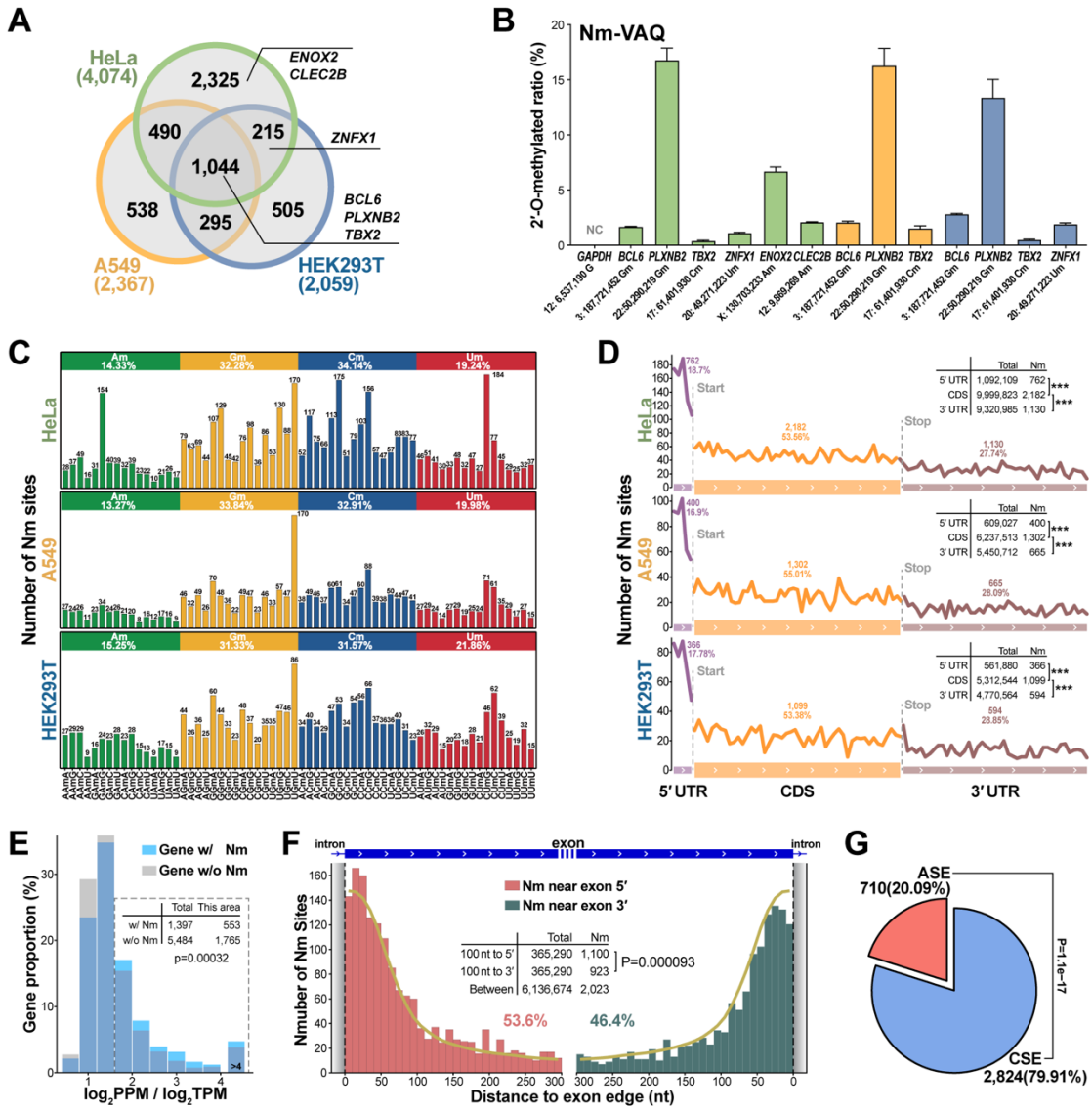

Figure 4 mRNA Nm sites in three human cell lines

(A) Overlap of mRNA Nm sites among the three cell lines by NJU-seq.

(B) The methylation status in mRNA Nm sites detected by Nm-VAQ. The Nm sites of HeLa, HEK293T, and A549 cells were presented as green, blue, and orange sites, respectively. The HeLa Nm sites' ratio data was the same as in Figure 4B. Error bars described SEM for three technical replicates.

(C) Methylated nucleotide frequency distribution of HeLa mRNA. Nm-1, Nm, and Nm+1 sites were considered tri-ribonucleotide units.

1044 (D) Distribution of HeLa Nm sites on a length-normalized mRNA transcript (see Methods).
1045 ***P < 0.001 (Pearson's chi-square test).

1046 (E) Translation efficiency of genes with and without Nm site(s) in HeLa. The ratio of protein
1047 abundance and RNA expression (log2PPM/log2TPM) represented translation efficiency. *P <
1048 0.05 (Pearson's Chi-square test).

1049 (F) Distribution of Nm sites near the exon 5′ (left) and exon 3′ (right) boundaries. All Nm sites
1050 were counted and divided into these two parts. The yellow dash represents the simulation of an
1051 even distribution.

1052 (G) Distribution of HeLa Nm sites in alternatively spliced exon (ASE) and constitutively
1053 spliced exon (CSE) regions. ***P < 0.001 (Pearson's chi-square test).

1054

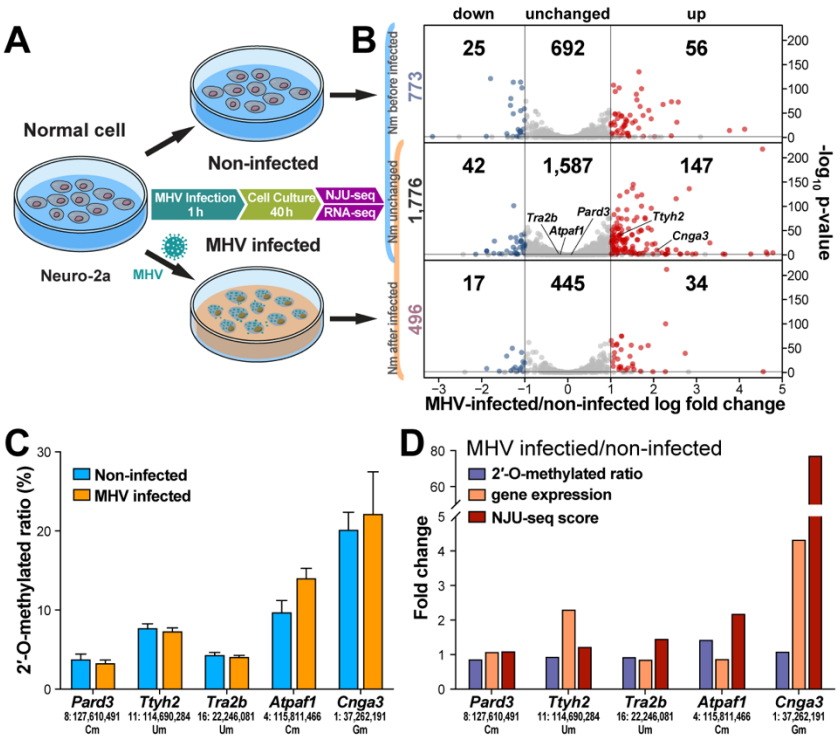

Figure 5 Dynamic 2′-O-methylation response to virus infection

(A) mRNA Nm sites changed in the Neuro-2a cell line after MHV infection. The flow of MHV infection was shown. Each of three MHV-infected and non-infected samples was performed with NJU-seq and RNA-seq.

(B) 773 non-infected-specific, 1,776 shared, and 496 MHV-infected-specific Nm sites were detected as shown left. Genes containing these Nm sites were identified as down-regulated, unchanged, and up-regulated according to RNA-seq.

(C) The 2′-O-methylated ratio of shared Nm sites detected by Nm-VAQ. Error bars described SEM for three biological replicates.

(D) Fold changes of the shared Nm sites' 2′-O-methylated ratio, NJU-seq score, and Nm-site-located genes' expression after MHV infection.

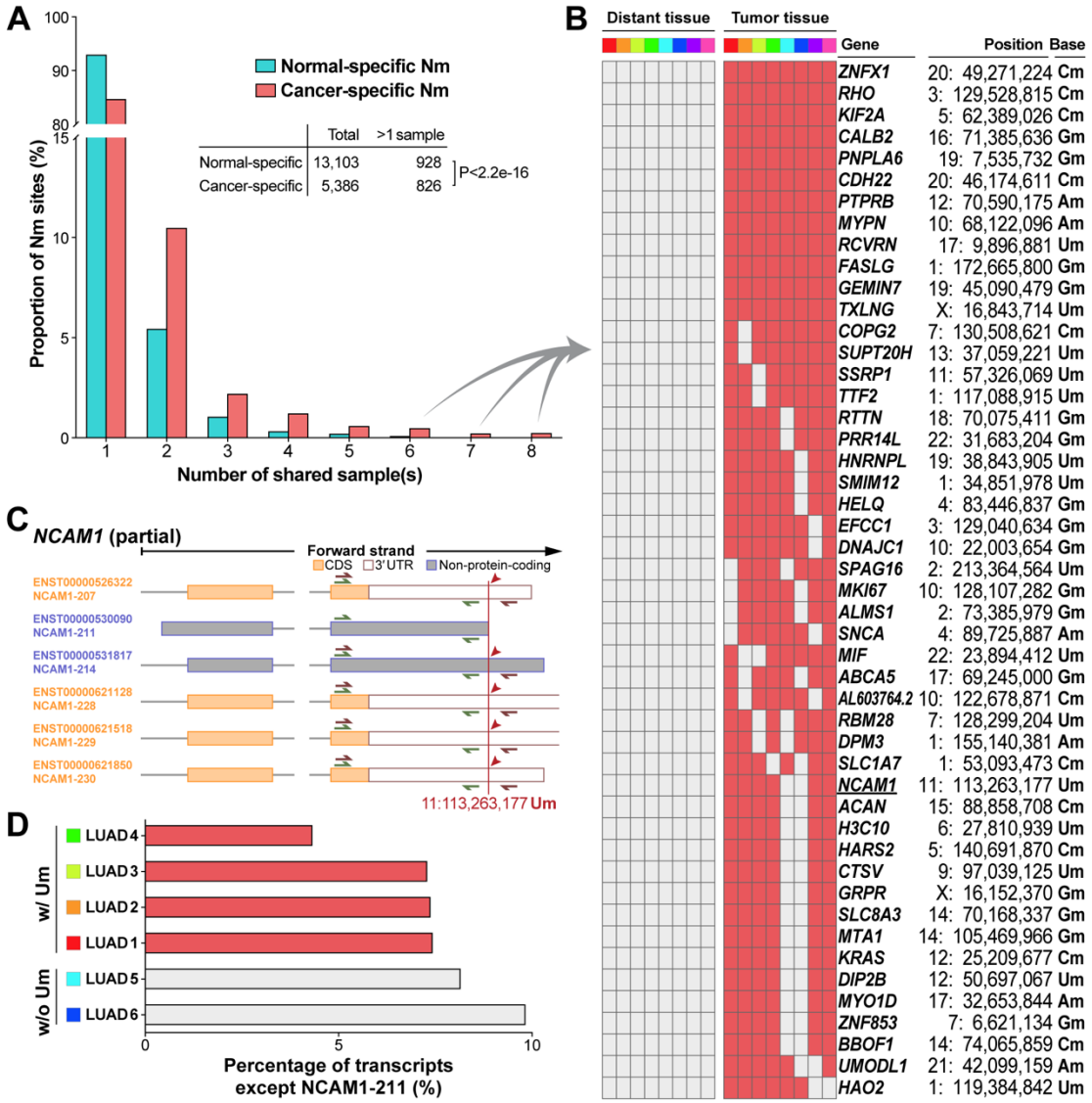

Figure 6 Significant different Nm patterns in normal and lung cancer tissues

(A) Sharing of specific Nm sites detected in lung cancer or normal tissue samples was shown. Eight pairs of tumor tissues and distant normal tissues from different lung cancer patients were sequenced and detected. Cancer-specific Nm sites occurred in at least one cancer tissue but were not detected in any normal tissue. The opposite is true for normal-specific Nm sites. The numbers of sites specific in over one cancer or normal tissue were subjected to the chi-square test.

(B) Specific mRNA Nm sites among over five lung cancer samples are listed.

1077 (C) Um site (11:113,263,177) on *NCAM1* was located at the 3′ end of the transcript NCAM1-
1078 211. The green or red arrows indicated the primers for six transcripts (NCAM1-207, 211, 214,
1079 228, 229, and 230) or five transcripts (without NCAM1-211) RT-qPCR amplification.

1080 (D) Percentage of transcripts except NCAM1-211. The proportion of the above five transcripts
1081 to six transcripts covering the Nm site was shown. Pastel red means Nm-detected, while gray
1082 means undetected.

1083

1084 Table 1 Comparison of 2′OMe-seq, RiboMethSeq, Nm-seq, and NJU-seq

Method	RiboMethSeq	2OMe-seq	Nm-seq	NJU-seq
Main principle	The property of resistance to alkaline hydrolysis of Nm site	Nm sites hinder reverse transcription at low dNTPs concentrations	Nm sites are specifically resistant to Oxidation and β -Elimination	MgR hydrolyzes RNA to the Nm+1 sites
identification Criteria for Nm sites	Negative signal	Positive signal	Positive signal	Positive signal
Methylation ratio	Yes	No	No	No
methylation copy number	No	No	Yes	Yes
RNA species	rRNA, tRNA	rRNA	rRNA, mRNA	All RNA species
Other	Requiring high sequencing coverage and high RNA counts.	Results are influenced by RNA secondary structure	RNA 3′ end 2′-O-methylation resulted less ligation efficiency than surrounding non-modified sites, producing false-positive results. Large amount of RNA was needed.	Without limitation by RNA secondary structure, other modifications, and costs.

1085

1086 Table 2 Comparisons of LC-MS, RTL-P, DNA polymerase, and Nm-VAQ methods

Method	LC-MS	RTL-P	DNA polymerase	Nm-VAQ
Main principle	Purification of RNA fragments containing modification sites and specific enzymatic hydrolysis to separate and analyze modification signal	2′-O-methylation induced reverse transcription stop at low dNTP concentrations	Am or Cm in 1nt downstream of the primer hindered the reverse transcription reaction	2′-O-methylation inhibited the cleavage of RNase H
Region/site-specific	Yes	No	No	Yes
Effective target	Am/Gm/Cm/Um	Am/Gm/Cm/Um	Am /Cm	Am/Gm/Cm/Um
Methylation ratio	Yes	No	Yes	Yes
absolute quantification of methylation copy number	No	No	No	Yes
Potential false result	No	Yes	Unknown	No
Other	Large amounts of high purity RNA, which is very laborious, are not suitable for detecting modifications of low abundance RNA	The methylation ratio varied significantly with the different RNA expression		Precise quantification of Nm ratio and methylation copy numbers at unknown RNA concentrations

1087